1.E.1:2.H

Nuclear Physics **A192** (1972) 449—495; © *North-Holland Publishing Co., Amsterdam*
Not to be reproduced by photoprint or microfilm without written permission from the publisher

REORIENTATION MEASUREMENTS USING THE DOPPLER-SHIFT METHOD: STATIC QUADRUPOLE MOMENTS OF ^{20}Ne, ^{22}Ne, ^{24}Mg, ^{26}Mg AND ^{28}Si †

D. SCHWALM

I. Physikalisches Institut der Universität Heidelberg, 69 Heidelberg, W. Germany

and

Brookhaven National Laboratory, Upton, New York 11973,

A. BAMBERGER, P. G. BIZZETI †† and B. POVH

Max-Planck Institut für Kernphysik in Heidelberg, 69 Heidelberg, W. Germany

and

G. A. P. ENGELBERTINK ‡, J. W. OLNESS and E. K. WARBURTON

Brookhaven National Laboratory, Upton, New York 11973

Received 29 May 1972

Abstract: The static quadrupole moments of the first excited $I^{\pi} = 2^{+}$ states in ^{20}Ne, ^{22}Ne, ^{24}Mg, ^{26}Mg and ^{28}Si were measured via the reorientation effect observed in Coulomb excitation with beams of ^{32}S, ^{34}S and ^{37}Cl ions. The quadrupole moments were deduced from the Doppler-broadened γ-ray lineshapes observed at 0° with respect to the beam by means of a Ge(Li) detector. The results are: $Q(^{20}\mathrm{Ne}, 2^{+}) = -0.23 \pm 0.08$ $e \cdot$b, $Q(^{22}\mathrm{Ne}, 2^{+}) = -0.18 \pm 0.04$ $e \cdot$b, $Q(^{24}\mathrm{Mg}, 2^{+}) = -0.24 \pm 0.06$ $e \cdot$b, $Q(^{26}\mathrm{Mg}, 2^{+}) = -0.16 \pm 0.04$ $e \cdot$b (-0.12 ± 0.04 $e \cdot$b), and $Q(^{28}\mathrm{Si}, 2^{+}) = +0.17 \pm 0.05$ $e \cdot$b. Two values are quoted for ^{26}Mg corresponding to the two possible signs of an interference term arising from virtual excitations through the second excited 2^{+} state of ^{26}Mg. A detailed description of the experimental technique and analysis is given, including the procedure whereby the semi-classical analysis of experimental lineshapes is modified to accord with a full quantal treatment of Coulomb excitation. Perturbing effects due to virtual E1 excitations and deorientation effects are calculated and found to be small.

E

NUCLEAR REACTIONS ^{20}Ne, ^{22}Ne, ^{24}Mg, (^{32}S, ^{32}S'), $E = 41$–55 MeV, ^{26}Mg (^{37}Cl, ^{37}Cl'), $E = 51$–54 MeV, ^{28}Si(^{34}S, ^{34}S'), $E = 54$ MeV; measured $\sigma(E_{\gamma})$. ^{20}Ne, ^{22}Ne, ^{24}Mg, ^{26}Mg, ^{28}Si levels deduced Q. Coulomb excitation, reorientation measurement.

1. Introduction

The observation of the reorientation effect [1,2]) in Coulomb excitation allows the determination of the size and the sign of static quadrupole moments of excited nuclear states. Although the method itself was suggested many years ago [1]), its applicability

† Work partially supported by the US Atomic Energy Commission.

†† Present address: Università di Firenze, Firenze, Italy.

‡ Present address: Robert Van de Graaff Laboratory, University of Utrecht, The Netherlands.

especially in light nuclei was strongly connected to the development of accelerators with suitable heavy-ion beams. During the past decade experiments were concentrated primarily on the measurement of quadrupole moments of the first 2^+ states of medium and heavy even-mass nuclei, utilizing projectiles with $A \leqq 16$. A considerable body of data has thus been acquired on the systematic behavior of the nuclear shape. For lighter target nuclei, however, measurements of the Coulomb excitation process were hindered by direct competition from inelastic scattering of the light projectiles via specifically nuclear interactions. With the more recent advent of suitable heavy-ion beams, several groups [3-7]) have initiated measurements of the quadrupole moments of the first excited 2^+ states of even sd shell nuclei. In most of these studies the contribution of the reorientation effect to the Coulomb excitation process was deduced from the excitation probability via its characteristic dependence on the scattering angle of the projectile; the measurements differ only in the particular experimental techniques which were used. Only two measurements have been performed so far in light nuclei [Pelte *et al.* [4]) and Olsen *et al.* [7])] where the dependence of the angular distribution of the de-excitation γ-rays on the reorientation effect was used.

The influence of the reorientation effect on the excitation probability can be seen most easily if the Coulomb excitation process is treated in a second-order perturbation approach, although this description cannot be used for a quantitative analysis because of the strength of the interaction. In second order the excitation probability for a transition from a $I^\pi = 0^+$ to a $I^\pi = 2^+$ state in the target nucleus is given by [2])

$$P_{02}^{(1,2)}(\Theta_1) = P_{02}^{(1)}(\Theta_1)\left\{1+1.32\frac{A_1}{1+A_1/A_2}\frac{\Delta EQ(2^+)}{Z_2}K(\xi,\Theta_1)\right\}, \tag{1}$$

where all second-order terms other than the reorientation term have been neglected. In this expression A_1, A_2, and Z_1, Z_2 are the mass (in amu) and charge number of the projectile and target nucleus, respectively, and Θ_1 is the scattering angle of the projectile in the c.m. system. (The corresponding expression for projectile excitation is obtained by replacing Z_2 by Z_1.) The excitation energy of the $I^\pi = 2^+$ state is ΔE (MeV) and its static quadrupole moment is denoted by $Q(2^+)(e \cdot \mathrm{b})$; $P_{02}^{(1)}$ is the first-order excitation probability, which is proportional to the $B(\mathrm{E2}, 0 \to 2)$ value. The reorientation term (given by the second term in the brackets) is proportional to the static quadrupole moment $Q(2^+)$ of the 2^+ state and a function $K(\xi, \Theta_1)$, which does not depend significantly on the adiabaticity parameter ξ, i.e. on the projectile energy E_p, but strongly on the scattering angle Θ_1 of the projectile [2]). In the Coulomb excitation of light nuclei with heavy ions (such as ^{32}S, for example), the size of the reorientation term is typically of the order of $-25\,\%$ for $\Theta_1 = 180°$ and $-10\,\%$ for $\Theta_1 = 90°$ assuming a quadrupole moment of $Q(2^+) = -0.2\ e \cdot \mathrm{b}$.

It follows from eq. (1) that at least two independent measurements of the excitation probability are needed in order to deduce $Q(2^+)$ without introducing an additional error due to the uncertainty of the $B(\mathrm{E2}, 0 \to 2)$ value. In light nuclei the only practical choice is the measurement of the excitation probability at different scattering angles Θ_1 of the projectile.

The straightforward technique is the direct measurement of the intensity of the inelastic scattered particles relative to that of the elastic ones. Although in principle very simple, the extraction of the excitation probability with an accuracy necessary to determine the relatively small reorientation effect is quite difficult, because the inelastically scattered projectiles must be detected in the presence of the much more intense elastic scattering. In this respect the limited energy resolution of available particle detectors and the purity of the target material present serious restrictions. Several approaches have been taken in attempts to overcome these difficulties.

Vitoux *et al.* [6]) measured the scattered projectiles in coincidence with the recoiling nuclei, where the former were observed in a position sensitive detector. From the angle-energy relations imposed by the kinematics they were thus able to obtain an additional degree of separation between the elastic and inelastically scattered particles.

Another way to reduce these difficulties is to observe the inelastic scattered projectiles or the recoiling target nuclei in coincidence with the de-excitation γ-rays. Häusser *et al.* [4]) used either one particle detector at a forward angle to detect the scattered particles as well as the recoiling target nuclei (corresponding to projectiles scattered in the backward direction) or two particle detectors, one at forward and one at a backward angle, in coincidence with the γ-rays observed in one of an array of several NaI detectors. A similar technique was applied by Nakai *et al.* [5]) in their work on projectile excitation. Here the projectiles were observed at two different angles in coincidence with a single NaI crystal placed at 55°. In this type of experiment, however, the particle-γ correlation is measured rather than the particle distribution. It is therefore necessary to consider explicitly the extent to which the initial nuclear alignment, produced via the Coulomb excitation process, is retained during the lifetime of the nuclear state. It is known that nuclei recoiling out of the thin target into vacuum are highly ionized and the strong magnetic field produced at the nucleus by unpaired electrons can bring about a fast attenuation of the angular correlation (deorientation effect) [refs. [8, 9])].

In the method described in the present paper the de-excitation γ-rays are observed at 0° with respect to the beam by means of a high-resolution Ge(Li) detector. Using a thin target such that the excited nuclei recoil into vacuum with essentially negligible energy loss, the observed Doppler shifts determine uniquely the scattering angle of the associated projectiles. Thus, from a single measurement of the γ-lineshape at 0° the angular correlation for γ-emission at 0° and *all* scattering angles of the inelastic projectiles between 0° and 180° can be obtained simultaneously, provided that the detector resolution is adequate to allow a true measure of the spectral shape. Here we are aided by the large recoil velocities which result from heavy-ion Coulomb excitation. For example, in the case of ^{24}Mg excited by 48 MeV ^{32}S ions, the line width of the 1369 keV transition in ^{24}Mg is $\approx$ 80 keV, which is large compared to the Ge(Li) detector resolution of $\approx$ 2–3 keV.

In the following we report the results of our measurements on the quadrupole moments of the first 2^+ states of ^{20}Ne, ^{22}Ne, ^{24}Mg, ^{26}Mg and ^{28}Si together with a detailed theoretical description of the method and analysis of the individual experiments. Three of these measurements (^{20}Ne, ^{22}Ne, ^{24}Mg) have been published already in a short form [3]); they are included here since the more complete theoretical description which we shall present allows a more precise interpretation of the experimental data.

The derivation of the γ-ray lineshape for the present geometry is given in sect. 2, together with a discussion on the validity of the semiclassical treatment of the Coulomb excitation process, as opposed to a full quantal treatment. Furthermore, possible effects due to excitations via high-lying states, especially the giant dipole states, are considered and the modification of the γ-lineshape due to the deorientation effect is discussed. In sect. 3 the experimental procedure is described while in sect. 4 the analysis of the measurements and the results are presented. In sect. 5 our results are compared with those obtained in experiments using alternative techniques, and also with various theoretical predictions.

2. Theoretical considerations

2.1. DERIVATION OF THE γ-LINESHAPE

For detection of de-excitation γ-rays at $\theta_\gamma = 0°$ with respect to the beam, the γ-lineshape can be easily calculated if we include only the first-order dependence on the nuclear velocity. In this case the Doppler shift ΔE_γ is given by

$$\Delta E_\gamma = E_\gamma - E_{\gamma 0} = E_{\gamma 0} v_z , \tag{2}$$

where $E_{\gamma 0}$ is the de-excitation energy and v_z is the projection of the recoil velocity $\boldsymbol{v}$ of the excited target nucleus on the beam axis. (Throughout this paper all velocities are measured in units of the velocity of light.) The relationship, in the c.m. system, between the recoil angle Θ_2 of the target nucleus and the corresponding scattering angle Θ_1 of the projectile is simply $\cos\Theta_1 = -\cos\Theta_2$. Thus we can write

$$v_z = v_{\mathrm{c.m.}} - v_{\mathrm{s}2}\cos\Theta_1 , \tag{3}$$

where $v_{\mathrm{c.m.}}$ and $v_{\mathrm{s}2}$ are the velocities of the c.m. and of the recoiling target nucleus in the c.m. system, respectively. The one-to-one relation between the scattering angle Θ_1 and the Doppler shift follows directly from eqs. (2) and (3).

The cross section for γ-emission at $\theta_\gamma = 0°$ after Coulomb excitation from the $I^\pi = 0^+$ state to an $I^\pi = 2^+$ state is given by [10])

$$\frac{\mathrm{d}\sigma_\gamma(\Theta_1)}{\mathrm{d}\Omega_1} = \frac{\mathrm{d}\sigma_{\mathrm{R}}(\Theta_1)}{\mathrm{d}\Omega_1} \times \sum_{k=0,2,4} \alpha_{k0}(\Theta_1) F_k(2,2,0,2)\sqrt{2k+1}\,\frac{\Delta\Omega_\gamma}{4\pi} , \tag{4}$$

where $\mathrm{d}\sigma_{\mathrm{R}}/\mathrm{d}\Omega_1$ is the Rutherford cross section and F_k are the usual γ-γ correlation coefficients [11]). The statistical tensor $\boldsymbol{\alpha}$ contains the information on the Coulomb-excitation process with α_{00} being identical to the excitation probability P_{02}. The tensor α can be obtained from the computer code of Winther and de Boer [10]). In this program the excitation amplitudes are calculated in the semiclassical approach by solving the time-dependent coupled differential equations in these amplitudes numerically.

The γ-lineshape observed at 0° with respect to the beam is then found to be given by

$$\frac{\mathrm{d}n(\Delta E_\gamma)}{\mathrm{d}\Delta E_\gamma} = \frac{2\pi}{E_{\gamma 0} v_{s2}} \frac{\mathrm{d}\sigma_\gamma(\Theta_1(\Delta E_\gamma))}{\mathrm{d}\Omega_1}, \tag{5}$$

where the integration over the projectile azimuth ϕ_1, i.e. over all scattered particles causing the same Doppler shift, has been carried out. Eq. (5) demonstrates the direct correspondence between the γ-lineshape and the Coulomb excitation cross section with respect to dependence upon the scattering angle Θ_1.

The general formula for the γ-lineshape is derived in appendix A. 1 for an infini-

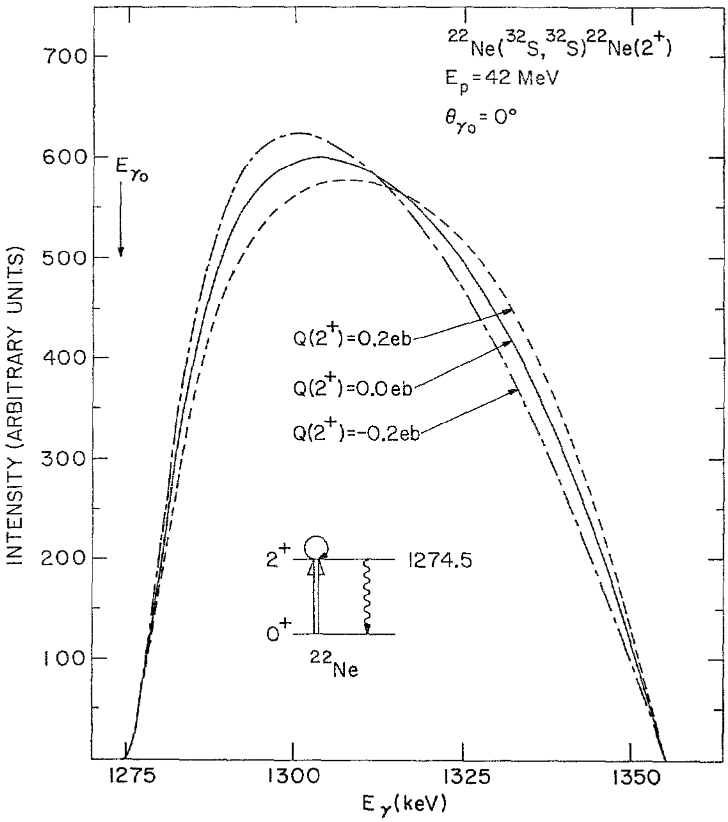

Fig. 1. Calculated lineshapes for the ^{22}Ne 1275 keV γ-ray resulting from Coulomb excitation in a thin ^{22}Ne target bombarded with 42 MeV ^{32}S ions. A 30 cm^3 Ge(Li) detector was assumed to be located at a distance of 5 cm from the target at $\theta_{\gamma 0} = 0°$. The three lineshapes are normalized to have the same intensity.

tesimally thin target. In this derivation the relativistic transformation of the γ-ray from the rest system of the emitting nucleus into the lab system is carried out to second order in v and the finite solid angle of the γ-detector is taken into account. Fig. 1 shows the γ-lineshape thus calculated for Coulomb excitation of the first excited $I^\pi = 2^+$ state of ^{22}Ne with 42 MeV ^{32}S ions. The calculation was done for a 30 cm^3 Ge(Li) detector located at a distance of 5 cm from the target at $\theta_{\gamma 0} = 0°$ and assumes $B(\mathrm{E2}, 0 \to 2) = 0.020\ e^2 \cdot \mathrm{b}^2$. Since we are not measuring absolute γ-intensities, the area of the three γ-lineshapes calculated with $Q(2^+) = 0$ and $Q(2^+) = \pm 0.2\ e \cdot \mathrm{b}$ are normalized to have the same area. The influence of the reorientation effect on the γ-lineshape is reflected in a change of the curvature at medium Doppler shifts. The γ-intensity at maximum Doppler shifts vanishes in this geometry because for back scattered particles only the $m = 0$ substate can be populated.

As suggested by the second-order perturbation approach [eq. (1)] the form of the γ-ray line is not sensitive to the $B(\mathrm{E2})$ value. Assuming $B(\mathrm{E2}, 0 \to 2) = 0.034\ e^2 \cdot \mathrm{b}^2$ and $Q(2^+) = 0.2\ e \cdot \mathrm{b}$, the form of the calculated γ-lineshape is indistinguishable from the corresponding curve shown in fig. 1; the actual differences are $< 1\ \%$.

The influence of the target thickness (typically 100–300 μg/cm^2) on the γ-lineshape is discussed in appendix A. 2. Two effects are considered: (i) The energy loss of the projectiles in the target, which was taken into account by integrating the γ-lineshape over the different beam energies, and (ii) the slowing-down process of the excited recoil nuclei in the target. For the particular case of 48 MeV ^{32}S ions impinging on a 150 μg/cm^2 thick ^{24}Mg target, where the effect is largest as compared to the other measurements presented in this paper, the slowing down of the excited ^{24}Mg nuclei, assuming $\tau = 2.0$ psec for the lifetime of the 2^+ state, results mainly in a shift of the γ-lineshape by about -1.5 keV. The errors involved in these corrections to the γ-lineshape due to uncertainties in the lifetime, target thickness, and specific energy-loss curve are small and are discussed for each measurement in sect. 4.

2.2. QUANTAL CORRECTIONS

Because of the considerable computational difficulties involved in an exact quantal treatment of the Coulomb excitation, the reorientation effect is normally calculated using the semiclassical approach, in which the projectile is assumed to move on a classical trajectory which is symmetrized in the velocities of the incoming and outgoing projectile. This is supposed to be a good approximation if the Sommerfeld parameter η is very large compared to unity, η being the ratio of the half-distance of closest approach to the de Broglie wave length of the projectile.

The divergence between semiclassical (SC) and quantal (QM) treatments of the Coulomb excitation process have been thoroughly investigated [12,13]) for the case where only two states are involved in the excitation process, namely the $I^\pi = 0^+$ ground state and the first $I^\pi = 2^+$ state. Differences were found to be proportional to η^{-1} and to introduce, in most practical cases, an uncertainty of about 5–10 % in the quadrupole moments obtained from semiclassical analyses of data.

The quantal corrections for our experiments were calculated from the results of Smilansky [12]) for 18.5 MeV ^{16}O on ^{22}Ne, which is the example closest to our conditions, and using interpolation procedures deduced from the work of Alder and Pauli [ref. [13])].

For $\theta_\gamma = 0°$ the γ cross section obtained in the exact quantal treatment can be written again in the form of eq. (4), with α_{k0} being replaced by $\alpha_{k0}^{\mathrm{QM}}$. The latter were obtained by correcting the tensor elements $\alpha_{k0}^{\mathrm{SC}}$, calculated in the Winther-de Boer program, by means of eq. (6),

$$\alpha_{00}^{\mathrm{QM}} = \alpha_{00}^{\mathrm{SC}} - \Delta S \alpha_{00}^{\mathrm{SC}}(Q = 0), \tag{6a}$$

$$\alpha_{k0}^{\mathrm{QM}} = \alpha_{k0}^{\mathrm{SC}}(\alpha_{00}^{\mathrm{QM}}/\alpha_{00}^{\mathrm{SC}}) + \Delta b_k \sqrt{5}\alpha_{00}^{\mathrm{QM}}, \tag{6b}$$

for $k = 2, 4$. The quantal corrections ΔS and Δb_k are related to the sensitivity function S and the particle parameter b_k defined in ref. [12]) by

$$\Delta S = S^{\mathrm{QM}} - S^{\mathrm{SC}}, \tag{7a}$$

$$\Delta b_k = b_k^{\mathrm{QM}} - b_k^{\mathrm{SC}}, \tag{7b}$$

for $k = 2, 4$. Eq. (6a) is based on the observation that for $\eta \geqq 4$ and $Q(2^+) = 0$ differences between the semiclassical results and those obtained in quantal calculations are negligible [12, 13]). The quantal corrections ΔS and Δb_k are in general functions of four parameters which describe uniquely the Coulomb excitation process, namely the Sommerfeld parameter η, the adiabaticity parameter ξ, and the two coupling parameters χ_{02} and χ_{22}, which are proportional to $(B(\mathrm{E2}, 0 \to 2))^{\frac{1}{2}}$ and $Q(2^+)$, respectively. For the symmetrized definition of η, ξ, χ_{02} and χ_{22} see ref. [2]).

In fig. 2 ΔS, Δb_2 and Δb_4 are displayed for 18.5 MeV ^{16}O ions impinging on ^{22}Ne. The corresponding QM γ-lineshapes are shown in fig. 3. These lineshapes were well reproduced (i.e. fitted) using the semiclassical theory, with the quadrupole moment and the normalization treated as variables. We define the quantal correction ΔQ by

$$\Delta Q = Q(2^+) - Q^{\mathrm{SC}}, \tag{8}$$

where Q^{SC} is the quadrupole moment obtained in the semiclassical analysis. For the case shown in fig. 3, we obtain $\Delta Q = +0.076\ e \cdot \mathrm{b}$ and $\Delta Q = +0.071\ e \cdot \mathrm{b}$ for $Q(2^+) = 0$ and $Q(2^+) = -0.156\ e \cdot \mathrm{b}$, respectively.

The same method was used to calculate ΔQ for the measurements presented in this paper. The quantal corrections ΔS and Δb_k were interpolated from those shown in fig. 2 using their known dependence on η, ξ, χ_{02} and χ_{22}. The results are compiled in table 1. In all cases the QM γ-lineshapes were well reproduced by those calculated in the semiclassical treatment. Therefore, the analyses of the experiments were carried out using the semiclassical theory; the values Q^{SC} thus obtained were later corrected by means of table 1. The error in ΔQ due to the somewhat arbitrary extrapolation of Δb_k for $\Theta_1 \leqq 40°$, and due to our computational method of comparing the QM and

SC γ-lineshapes for $\theta_\gamma = 0°$ (and thus neglecting the finite solid angle of the γ-detector) is of the order of 10 %.

2.3. INFLUENCE OF HIGHER-LYING STATES

The contribution to the excitation probability of the first excited 2^+ state from virtual excitations via higher-lying states can be easily included in the computer code of Winther and de Boer [10]), if the size and relative phases of the matrix elements are known.

The states considered in detail were the second excited 2^+ and first 4^+ state. In all

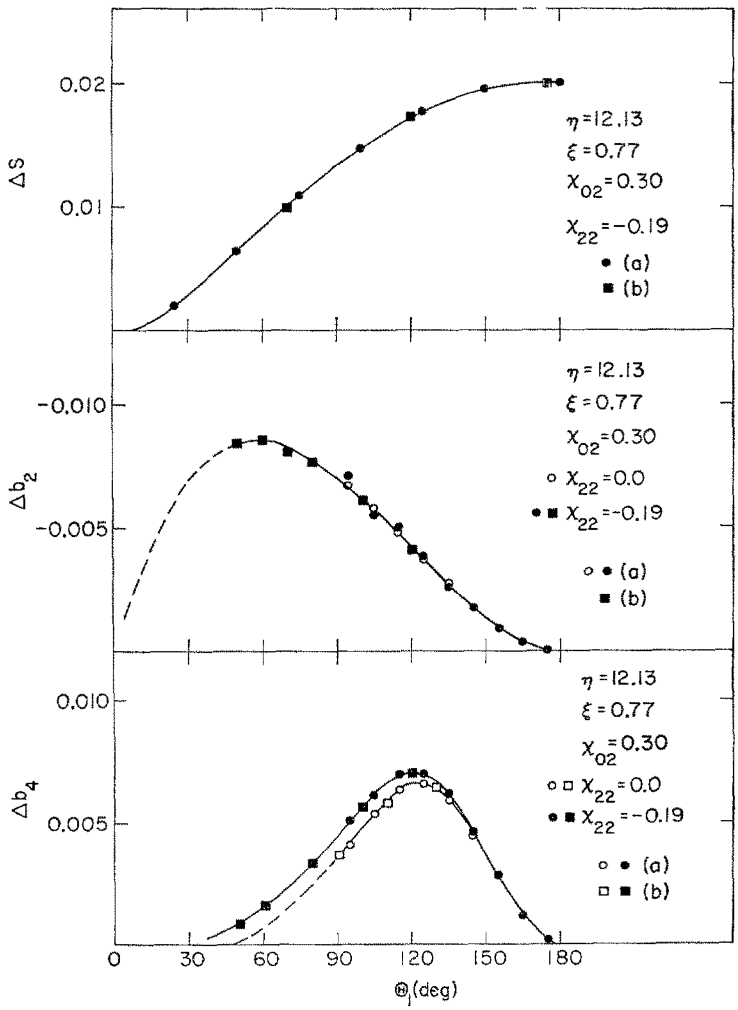

Fig. 2. The quantal corrections of the statistical tensor elements α_{00}, α_{20} and α_{40} for the special case of 18.5 MeV ^{16}O ions impinging on a ^{22}Ne target. For the definition of ΔS and Δb_k see main text. The points were either taken from ref. [12]) (a) or interpolated from ref. [13]) (b).

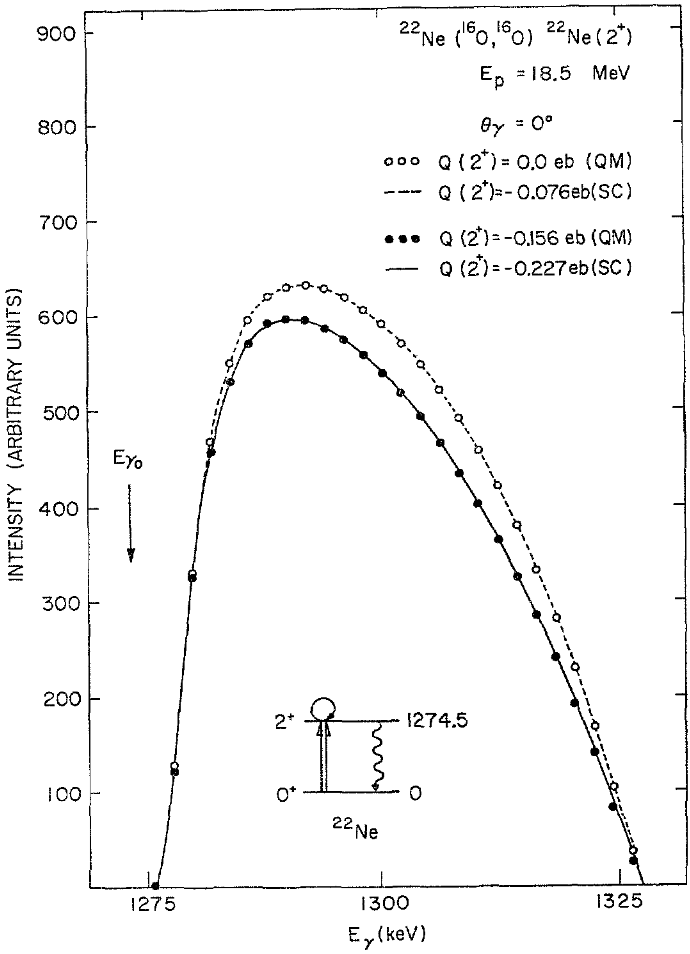

Fig. 3. A comparison of semiclassical and quantal analyses of the γ-lineshape, illustrating the extent to which the value of the extracted quadrupole moment depends on the quantal corrections. The points represent the lineshapes calculated with statistical tensors which were corrected for the quantal effects as discussed in the main text. The solid and dashed lines are the best fits obtained by using semiclassical calculated lineshapes and varying the quadrupole moment and the normalization.

cases discussed here with the exception of ^{26}Mg, the neglect of these corrections introduces an uncertainty in $Q(2^+)$ of less than $\pm 2\,\%$. In ^{26}Mg the second 2^+ state has a relatively low excitation energy, 2.9 MeV as compared to 1.8 MeV for the first excited 2^+ state, and was therefore included explicitly in the analysis.

The contribution from the virtual E1 excitation via the giant dipole resonance is more difficult to estimate because of lack of experimental information. In second-order perturbation theory the E1 contribution is given by eq. (57) of ref. [2]),

$$\frac{P_{02}^{(1,2)}(\mathrm{E1})}{P_{02}^{(1)}} = -119.8\,\frac{E_{\mathrm{p}}\sigma_{-2}\eta_0 e}{(1+A_1/A_2)Z_2}\langle 0^+||M(\mathrm{E2})||2^+\rangle^{-1}\Phi(\Theta_1, \xi), \tag{9}$$

TABLE 1

The quantal corrections ΔQ for quadrupole moments obtained in a semiclassical analysis of the γ-lineshapes

Target	Projectile	E_p (MeV)	ΔE (MeV)	$B(\mathrm{E2}, 0 \to 2)$ $(e^2 \cdot \mathrm{b}^2)$	$Q(2^+)$ $(e \cdot \mathrm{b})$	η	ξ_{02}	χ_{02}	χ_{22}	ΔQ $(e \cdot \mathrm{b})$
^{22}Ne	^{16}O	18.5	1.275	0.030	0.0	12.1	0.77	0.30	0.0	+0.076
					−0.156				−0.19	+0.071
^{20}Ne	^{32}S	40.0	1.634	0.029	0.0	23.2	1.31	0.29	0.0	+0.034
					−0.230				−0.28	+0.031
^{22}Ne	^{32}S	40.0	1.275	0.020	0.0	23.1	0.94	0.28	0.0	+0.032
					−0.170				−0.24	+0.030
^{24}Mg	^{32}S	48.0	1.369	0.043	0.0	25.2	0.87	0.42	0.0	+0.030
					−0.230				−0.34	+0.030
^{26}Mg	^{37}Cl	50.6	1.809	0.030	0.0	28.2	1.28	0.35	0.0	+0.021
					−0.100				−0.14	+0.020
^{28}Si	^{34}S	52.0	1.779	0.032	0.0	29.2	1.15	0.34	0.0	+0.020
					+0.150				+0.21	+0.023

Results are shown for two assumed values of $Q(2^+)$.

after correction for printing errors. The function $\Phi(\Theta_1, \xi)$ is defined in eq. (58) of ref. [2]). The properties of the giant resonance are contained in the two parameters σ_{-2} and η_0. The (-2) moment of the photonuclear absorption cross section is experimentally determined to be $\sigma_{-2} \approx 2.6A^{\frac{5}{3}}$ μb/MeV for nuclei in the sd shell [14]). The coupling of the ground state and the first excited state via the giant dipole states is given by η_0, which is defined as

$$\eta_0 = \sqrt{\frac{2}{5}} \frac{\sum_n \Delta E_n^{-1} \langle 0^+ || M(\mathrm{E1}) || n \rangle \langle n || M(\mathrm{E1}) || 2^+ \rangle}{\sum_n \Delta E_n^{-1} \langle 0^+ || M(\mathrm{E1}) || n \rangle \langle n || M(\mathrm{E1}) || 0^+ \rangle}, \tag{10}$$

where n labels any giant dipole state and ΔE_n is its excitation energy. In light nuclei there is no experimental data available which allows a reliable determination of η_0.

To date all theoretical estimates of η_0 are based essentially on the hydrodynamic model, where the giant dipole resonance is described as being due to the oscillations of protons and neutrons along the main intrinsic axis of the nucleus. Assuming a deformed axially symmetric nucleus and describing the 0^+ and 2^+ states as the lowest members of the ground state rotational band, MacDonald [15])† obtained

$$\eta_0 = \frac{2}{\sqrt{5}} \frac{1-(\Delta E_{K=0}/\Delta E_{K=1})^2}{1+2(\Delta E_{K=0}/\Delta E_{K=1})^2}, \tag{11}$$

where $\Delta E_{K=0}$ and $\Delta E_{K=1}$ are the energies of the intrinsic dipole states corresponding to the oscillations along $(K = 0)$ and perpendicular to $(K = 1)$ the symmetry axis. For heavy deformed nuclei one obtains $\eta_0 \approx 0.2$ using the observed ratio of $\Delta E_{K=0}/$

† The value quoted in this letter has to be multiplied by a factor of $\sqrt{5}$ to read correctly.

$\Delta E_{K=1} \approx 0.75$. Similar values of $\eta_0 \approx 0.2$–0.3 are obtained for heavy deformed nuclei using the dynamic collective model [16]). In spherical nuclei one does not expect η_0 to be larger than in deformed nuclei [15]). This was verified by Douglas and MacDonald [17]) for medium heavy nuclei; using the dynamic collective model they obtained $\eta_0 \approx 0.1$–0.2.

The applicability of these estimates of η_0 to light nuclei is not quite obvious. While for nuclei above $A \approx 50$ the hydrodynamic model (or its more refined version, the dynamic collective model) gives a reasonable description of the gross structure of the giant dipole resonance as observed in the γ-absorption cross section, for nuclei below $A \approx 50$ the single-particle character of the giant dipole resonance becomes more and more important, which leads to deviations from the predictions of the collective models. However, for well-deformed nuclei such as ^{24}Mg, the observed [14]) giant dipole resonance has the same gross structure as in heavy deformed nuclei with $\Delta E_{K=0}/\Delta E_{K=1} \approx 0.75$ and a γ-absorption cross section of $\sigma_\gamma(K=0) : \sigma_\gamma(K=1) \approx 1:2$ as predicted in the hydrodynamic model. Calculations for ^{24}Mg including particle-hole excitations show, indeed, that the lower group contains mainly $K = 0$ states whereas in the higher group the $K = 1$ states are dominant [18]).

Another method to estimate the virtual E1 excitation results from its interpretation as a polarization effect [2,19]). Describing the nucleus as a uniformly charged body whose shape is given by $R_2 = R_{20}(1+\sum_\mu \alpha_{2\mu} Y_{2\mu})$, and assuming the nuclear polarizability tensor to be diagonal in the intrinsic system of the nucleus with principal polarizabilities proportional to the square of the radii in these directions, as suggested by the hydrodynamic model, the effective quadrupole operator is found to be given by

$$H^{(2)}_{\text{eff}} = H^{(2)}\left(1 - q\frac{a}{r}\right). \tag{12}$$

Here $H^{(2)}$ is the usual quadrupole operator [10]), r is the distance between the centers of the two colliding nuclei while a is the half-distance of closest approach in a head-on collision. The parameter q is related to the polarizability and thus to the σ_{-2} moment by

$$q = \frac{5}{3}\frac{\hbar c}{2\pi^2}\sigma_{-2}\frac{Z_1}{Z_2 a R_{20}^2}, \tag{13}$$

if target excitation is considered. (For projectile excitation Z_1 must be replaced by Z_2 and Z_2, R_{20} by Z_1, R_{10}, respectively.) Using the effective quadrupole interaction $H^{(2)}_{\text{eff}}$ in the perturbation approach to the Coulomb excitation process, the contribution of the dipole interaction to the excitation probability is again given by eq. (9) if one sets η_0 equal to

$$\eta_0 = \tfrac{4}{3}\sqrt{\pi}\,\frac{\langle 0^+||M(\text{E2})||2^+\rangle}{Z_2 e R_{20}^2}, \tag{14}$$

(eq. (65) of ref. [2]) after correcting for printing errors). The polarization description is valid for rotational and vibrational nuclei, but since the basic assumptions are the same as in the previous estimates, the same arguments hold for its applicability to the light nuclei.

Applying eq. (14) to the case of ^{24}Mg we obtain $\eta_0 \approx 0.3$, as compared to the value $\eta_0 \approx 0.2$ resulting from the previous estimate. It should be pointed out, however, that the estimate obtained by MacDonald [eq. (11)] is consistent with eq. (14) within the applied models, where the splitting of the giant dipole resonance is given approximately by

$$\frac{\Delta E_{K=0}}{\Delta E_{K=1}} \approx 1-\frac{3}{4}\sqrt{\frac{5}{\pi}}\,\beta_0 \approx 1-\sqrt{5\pi}\,\frac{\langle 0^+||M(\mathrm{E2})||2^+\rangle}{Z_2\,eR_{20}^2}\,. \tag{15}$$

The numerical difference between the two estimates is due partly to the fact that for ^{24}Mg the deformation parameter β_0 obtained from the splitting of the giant dipole resonance is smaller than that deduced from the B(E2) value.

In conclusion, it is felt that in the absence of experimental data on η_0, the influence of the virtual E1 excitation on the determination of quadrupole moments of light nuclei via the reorientation effect should be considered as an additional uncertainty rather than a well-known correction. To estimate these uncertainties for our experiments the polarization description was used which can be easily included in the Winther-de Boer program. Using lineshapes calculated with and without dipole polarization is was found that, in all cases, the extracted quadrupole moments differ by not more than $\Delta Q(\mathrm{E1}) = 0.006\ e\cdot\mathrm{b}$. The final analysis of our data was therefore carried out with the possible effects of the dipole-polarization neglected but including ΔQ(E1) in the uncertainty attached to $Q(2^+)$.

2.4. SIMULTANEOUS TARGET-PROJECTILE EXCITATION

In all calculations presented so far the projectile is considered as a point charge. The influence of the multipole-multipole interaction on the Coulomb excitation process has been investigated by Häusser *et al.* [20]) and Eisenstein *et al.* [21]). The effect is negligible for all projectile-target combinations used in the present measurements.

2.5. SAFE BOMBARDING ENERGY

The probability of Coulomb excitation increases strongly with increasing projectile energy. Therefore, experiments are usually designed to utilize the highest possible bombarding energy consistent with the requirement that the excitation process be purely electromagnetic, i.e. that the contribution of nuclear interactions to the excitation probability is negligible as compared to the reorientation effect.

Experimental investigations for ^{16}O and ^{32}S ions on ^{60}Ni [ref. [22])], ^{16}O on ^{24}Mg [ref. [6])], and ^{35}Cl on ^{27}Al [ref. [23])] show that this requirement is fulfilled if the minimum distance of closest approach in head-on collisions, $2a$, is larger than 13.3 fm, 14.4 fm, $\approx$ 11.8 fm and 13.1 fm, respectively. Defining a surface distance d by [22])

$$2a = 1.6(A_1^{\frac{1}{3}}+A_2^{\frac{1}{3}})+d, \tag{16}$$

these values are well reproduced for d = 3.0 fm. We therefore consider the projectile energy to be safe if the distance of closest approach in the head-on collision is larger than the value given by eq. (16) with d = 3.0 fm.

2.6. DEORIENTATION EFFECT

In the derivation of the γ-lineshape in subsect. 2.1 we assumed that during the lifetime of the excited state no change of its alignment takes place. In the present geometry the excited nuclei recoil with velocities up to $v \approx 0.07$ either into gases or out of thin targets into vacuum and are therefore highly ionized throughout the lifetime of the excited state. The magnetic fields produced at the nucleus by strongly bound unpaired electrons are of the order of 100–300 MG (200 MG for a single $1s_{\frac{1}{2}}$ electron in ^{24}Mg) and cause a large magnetic hyperfine splitting. As a consequence, the alignment of the excited nucleus can change rapidly and the particle-γ correlation can thus be perturbed. Assuming a randomly oriented hyperfine interaction the deorientation results in an attenuation of the particle-γ correlation. Eq. (4) is then to be replaced by

$$\frac{\mathrm{d}\sigma_\gamma(\Theta_1)}{\mathrm{d}\Omega_1} = \frac{\mathrm{d}\sigma_\mathrm{R}(\Theta_1)}{\mathrm{d}\Omega_1} \times \sum_{k=0,2,4} G_k(v)\alpha_{k0}(\Theta_1)F_k\sqrt{2k+1}\,\frac{\Delta\Omega_\gamma}{4\pi}, \tag{17}$$

where $G_k(v)$ are the attenuation coefficients ($G_k \leqq 1$, $G_0 \equiv 1$).

In recent deorientation measurements [8, 9]) it was shown that for light nuclei recoiling into vacuum the observed deorientation can be accounted for with the assumption of a static, isotropic hyperfine interaction. It was further observed that for excited states with lifetimes around 1 psec the deorientation is caused mainly by unpaired $1s_{\frac{1}{2}}$ and $2s_{\frac{1}{2}}$ electrons. The attenuation coefficients can therefore be written as

$$G_k(v) = 1-\Delta G_k(v) = 1-\sum_{n=1,2} p_{ns}(v)\Delta G_k(ns), \tag{18}$$

with

$$\Delta G_k(ns) = \frac{k(k+1)}{(2I+1)^2}\,\frac{[\omega(ns)\tau]^2}{1+[\omega(ns)\tau]^2}. \tag{19}$$

Here τ is the lifetime of the excited state with spin I, $\omega(ns)$ is the hyperfine frequency associated with the $ns_{\frac{1}{2}}$ electron, and $p_{ns}(v)$ is the probability of finding an unpaired $ns_{\frac{1}{2}}$ electron. It was found that these probabilities can be deduced approximately from the known equilibrium charge state distribution using statistical considerations [8, 9]). This conclusion is felt to be valid as long as the target thickness is larger than the thickness necessary to reach the equilibrium distribution, which is $\approx$ 10–20 μg/cm^2 [refs. [24, 25])].

Fig. 4a shows the γ-lineshape for the decay of ^{24}Mg(2^+) following Coulomb excitation by 48 MeV ^{32}S ions, as calculated both with and without deorientation effects.

Here we have assumed $\tau = 2.0$ psec, $Q(2^+) = -0.23\ e \cdot \mathrm{b}$ and the nuclear magnetic moment of the $I^\pi = 2^+$ state to be $g = 0.5$. The charge state distributions used to calculate $p_{ns}(v)$ were obtained from an empirical formula given by Dmitriev *et al.* [26]). The deorientation effect is most pronounced at high Doppler shifts for two reasons:

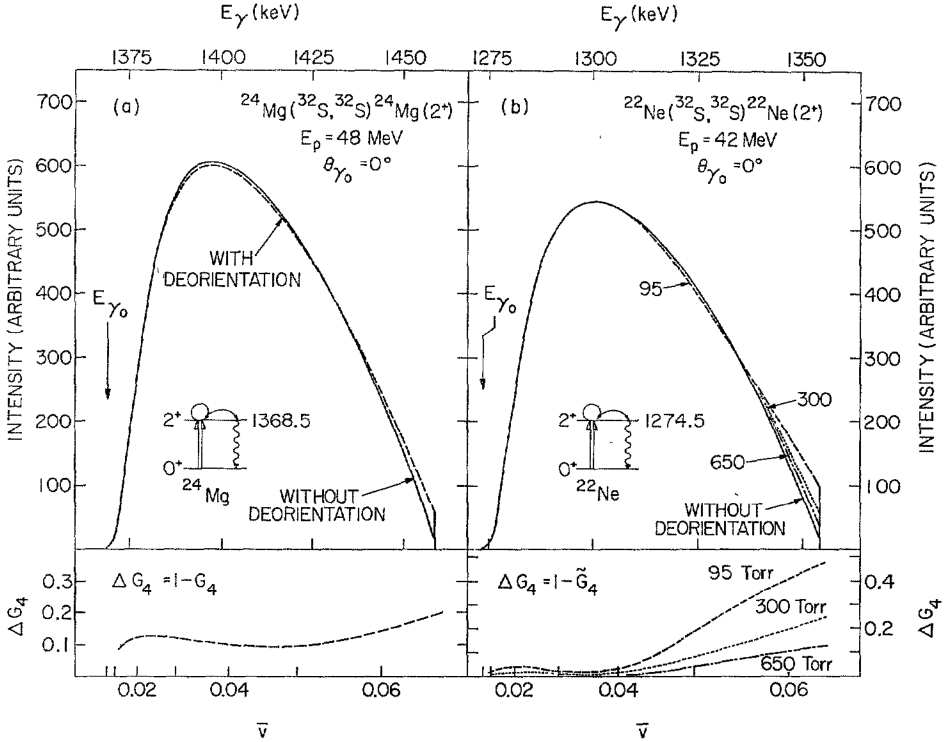

Fig. 4. Influence of the deorientation effect on the γ-lineshapes for a) recoil of ^{24}Mg(2^+) into vacuum and b) recoil of ^{22}Ne(2^+) into a ^{22}Ne gas at various pressures. The attenuation coefficients G_k and $\tilde{G}_k$ were calculated as discussed in the text.

(i) At recoil velocities above $v = 0.05$ the abundance of the $Z-1$ charge state increases strongly and thus also the probability for finding an unpaired $1s_{\frac{1}{2}}$ electron ($p_{1s}(0.065) \approx 0.2$). (ii) The emission of γ-quanta at 0° in coincidence with backscattered particles is now possible because substates with $m \neq 0$ have been populated by the hyperfine interaction after the excitation process.

For the ^{26}Mg and ^{28}Si measurements the influence of the deorientation effect on the γ-lineshape is smaller, mainly because the nuclear lifetimes are appreciably shorter than in the case of ^{24}Mg.

The reorientation measurements for ^{20}Ne(2^+) and ^{22}Ne(2^+) were performed using a gas target. In this case the electron configurations of the recoiling nuclei are changing rapidly in time due to the collisions between the moving ions and the gas atoms. The attenuation coefficients $\tilde{G}_k$ for a fluctuating hyperfine interaction were calculated using the formalism of Scherer [27]) (as corrected by Blume [28])). The basic assumption made here is that the direction of the atomic spin after the collision is randomly distributed. The attenuation coefficients are then found to be given by

$$\tilde{G}_k(v) = G_k(v, \lambda+\lambda_c)\left\{1+\frac{\lambda_c}{\lambda}(1-G_k(v, \lambda+\lambda_c))\right\}^{-1}, \tag{20}$$

where $G_k(v, \lambda+\lambda_c)$ is the attenuation factor for the static, isotropic hyperfine interaction as discussed above but calculated with $\lambda = \tau^{-1}$ replaced by $\lambda+\lambda_c = \tau^{-1}+\tau_c{}^{-1}$. The correlation time τ_c measures the mean time between two successive collisions. For $\tau_c \gg \tau$, $\tilde{G}_k$ reduces to the static value, while for $\tau_c \ll \tau$ and $(\omega\tau_c)^2 \ll 1$ the result of Abragam and Pound [29]) is obtained as shown in ref. [28]).

Thus far no experiments have been performed to measure the deorientation effect for light nuclei recoiling into a gas. We therefore assume that the probability of finding an unpaired $1s_{\frac{1}{2}}$ or $2s_{\frac{1}{2}}$ electron can be calculated again from the equilibrium charge state distributions as in the static case, and that the correlation time τ_c is proportional to the gas kinetic collision time,

$$\tau_c = \alpha(\pi(r_0+r_{\bar{Z}})^2 n_0 cvp/760)^{-1}. \tag{21}$$

Here r_0 and $r_{\bar{Z}}$ are the radii of the gas atoms and of the moving ions with mean charge $\bar{Z}$, respectively; c is the velocity of light, n_0 is the number of gas atoms per unit volume at normal conditions and p the gas pressure (Torr). The proportionality constant α should be of the order of 1 and was found to be $\alpha \approx 1.5$ for ^{22}Ne recoiling into ^{22}Ne (see subsect. 4.4). We would like to point out, however, that α enters eq. (20) as a free parameter and is therefore affected by the validity of all other assumptions as well. These assumptions are certainly quite rough because they imply that optical transitions are negligible and that the probabilities $p_{ns}(v)$ do not depend on the history of the moving ion.

In fig. 4b the γ-lineshape from the decay of ^{22}Ne(2$^+$) after Coulomb excitation with 42 MeV ^{32}S ions is shown as calculated with and without deorientation. The various parameters were set to be $\tau = 6.0$ psec, $Q(2^+) = -0.2\ e \cdot$ b, $g = 0.5$, $\alpha = 1$ and $p = 95$, 300 and 650 Torr. The charge state distributions were taken from ref. [26]). Again the main modification of the γ-lineshape occurs at Doppler shifts larger than $0.75\ \Delta E_{\gamma\max}$, but for smaller Doppler shifts and $p \gtrapprox 300$ Torr the influence of the deorientation effect on the γ-lineshape is very small. Thus we conclude that the reorientation measurements which were performed using a gas target are not affected by the details of the deorientation correction as long as we restrict ourselves to gas pressures of $p \gtrapprox 300$ Torr and that portion of the γ-lineshape for which $\Delta E_\gamma \lessapprox 0.75\ \Delta E_{\gamma\max}$.

3. Experimental procedure

A schematic view of the experimental set-up is shown in fig. 5. The heavy-ion beam enters a 2 cm diameter target chamber through a pair of Ta collimators, and after emerging from the target is stopped in a 0.5 mm thick Ta sheet. For the ^{20}Ne and ^{22}Ne measurements the chamber was replaced by a gas target which will be described in detail elsewhere [30]. In this case the beam entered the gas through a nickel window of about 500 μg/cm^2. The geometric thickness of the gas target was chosen to be large

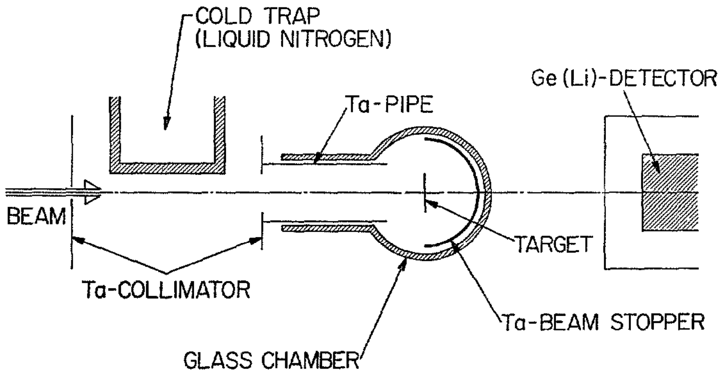

Fig. 5. Schematic view of the experimental set-up used in the measurements with solid targets.

compared to the mean flight path of the excited nuclei (10 mm as compared to $\tau v \lessapprox$ 0.02 mm and $\lessapprox$ 0.1 mm for ^{20}Ne and ^{22}Ne, respectively).

The ^{20}Ne, ^{22}Ne and ^{24}Mg experiments were performed using a 7^+ ^{32}S beam with energies between 42 and 55 MeV. The beam was supplied by the MP Tandem Van de Graaff of the Max-Planck Institut für Kernphysik in Heidelberg. The 6^+ ^{37}Cl and 6^+ ^{34}S beams of 54 MeV, which were used in the ^{26}Mg and ^{28}Si experiments, were produced by the second MP Tandem Van de Graaff of the three stage facility at the Brookhaven National Laboratory.

The de-excitation γ-rays were observed at 0° with respect to the beam by means of a Ge(Li) detector typically located at a distance of 5–7 cm from the target. The error in the angle alignment could be kept in the order of $\pm 3°$ by measuring the exact position of the Ge crystal in its aluminium housing with a collimated γ-ray source. The detector was shielded with lead bricks to suppress the target room background. All γ-ray spectra were recorded using a conversion gain of about 1 keV/channel in order to facilitate an accurate calibration; they were later contracted for further analysis by adding several channels together.

A typical γ-ray spectrum, obtained in the bombardment of a 260 μg/cm^2 thick ^{26}Mg target (99.4 % enriched) with 54 MeV ^{37}Cl ions is shown in fig. 6a. The target was evaporated onto a 110 μg/cm^2 thick Ni foil and was mounted in the target chamber with the Ni foil pointing upstream. The width of the γ-line, which originates from the in-flight decay of the first excited $I^\pi = 2^+$ state of ^{26}Mg, is about 115 keV as compared to the Ge(Li) detector resolution of 3.6 keV for 1.8 MeV γ-rays. The peak-to-background ratio is 10 : 1. The 1770 keV γ-ray line results from a weak ^{207}Bi source, which was mounted on the target chamber throughout the measurement to provide a reference line. For each reorientation measurement a set of control measurements was carried out to determine (i) the target thickness, (ii) the γ-ray background, (iii) the energy calibration of the γ-ray spectra and (iv) the properties of the Ge(Li) detector.

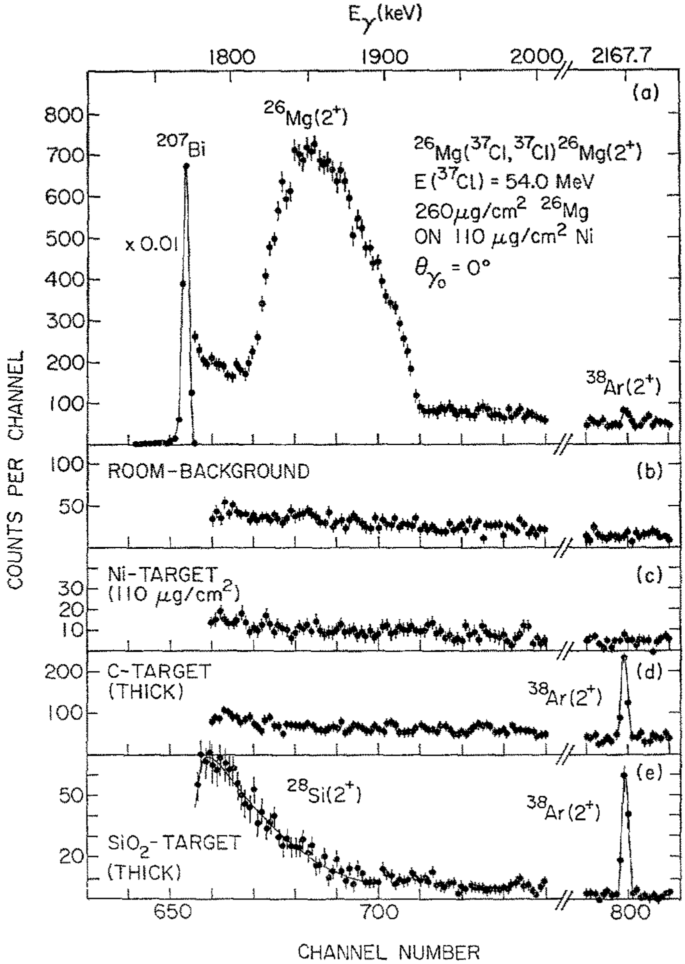

Fig. 6. a) Measured γ-ray spectrum from a thin ^{26}Mg target bombarded with 54 MeV ^{37}Cl ions. The target was evaporated onto a 110 μg/cm^2 thick Ni foil which pointed upstream. b) Gamma spectrum observed without beam. c) – e) Control spectra accumulated during the bombardment of a thin Ni-foil, a thick carbon and a thick oxygen target (chemical form SiO_2) with 54 MeV ^{37}Cl ions.

(i) The thickness of each solid target was determined by measuring the energy loss of the projectiles in the target. For the target used in the experiment shown in fig. 6a, for example, the total energy loss of 54 MeV ^{37}Cl ions was measured to be 6.17 ± 0.05 MeV. Separate measurements for the Ni foil, using a piece cut from the same sheet as the supporting foil, yielded a thickness of 1.35 ± 0.03 MeV corresponding to 110 ± 10

$\mu g/cm^2$. From these measurements the projectile energy after passing through the Ni backing is determined to be $E_p = 52.65 \pm 0.03$ MeV, while the energy loss in the ^{26}Mg target is $\delta E_p = 4.83 \pm 0.08$ MeV, which corresponds to a target thickness of 260 ± 30 $\mu g/cm^2$. The specific energy-loss curves used were calculated as described in refs. [23]) and [31]) (see also appendix A. 2).

The energy loss of the ^{32}S beam in the gaseous targets of ^{20}Ne and ^{22}Ne was calculated from the geometric target thickness, the gas pressure and the specific energy-loss curves. In the assumed error for δE_p the uncertainty in the number of atoms per unit volume due to the heating of the gas on the beam axis [32]) was included. The thickness of the entrance window of the gas cell was determined from its weight and also from the energy losses of 6 and 9 MeV α-particles.

(ii) Since we are measuring only singles spectra and the γ-lineshapes from Coulomb excitation are about 100 keV broad, possible sources of background must be studied carefully. For each measurement, therefore, it was necessary to determine the background contributions due to the target room, the Ta beam stopper, and possible contaminations of the target (namely carbon and oxygen) and of the foil supporting the target. In the lower part of fig. 6 the background spectra corresponding to the ^{26}Mg measurement shown in fig. 6a are displayed. All spectra were recorded using the same experimental set-up including the ^{207}Bi source. The spectrum shown in fig. 6c was obtained by bombarding a 110 $\mu g/cm^2$ thick Ni foil with 54 MeV ^{37}Cl ions. This spectrum, which includes possible contributions due to the Ta stopper, is not significantly different from the target room background shown in fig. 6b; most importantly, no structure is evident in the region of interest. The carbon and oxygen contributions were studied by bombarding thick targets of C and SiO_2 with 54 MeV ^{37}Cl ions. The ^{38}Ar line observed in both spectra and also weakly in fig. 6a is probably due to the β-decay of ^{38}Cl, which can be produced by transferring a neutron from carbon or oxygen to ^{37}Cl. Again in the region of interest neither carbon nor oxygen gives rise to background lines; the $^{28}Si(2^+)$ line is due to the Coulomb excitation of silicon present in the oxygen target. It should be pointed out that the origin of all significant background lines observed in the reorientation experiments reported here could be explained on the basis of background measurements similar to those described above.

(iii) The quadrupole moment extracted from the γ-lineshape is quite sensitive to the energy calibration of the γ-ray spectrum and to the exact value of the unshifted γ-energy $E_{\gamma 0}$($\Delta Q \approx \pm 0.01$ $e \cdot$ b for $\Delta E_{\gamma 0} = \pm 0.2$ keV). In order to minimize these possible systematic errors, in each measurement γ-rays from weak radioactive sources were recorded simultaneously. By using these calibration data together with those from well known background lines, e.g. the 2.6 MeV line of ThC″, the uncertainties in the calibration could be kept $\lessapprox \pm 0.1$ keV in the region of interest. The energies adopted for the calibration lines were taken from the compilation of Marion [33]) and recent measurements [34]). They are listed in table 2.

While the unshifted γ-ray energies for the decay of the first excited states of ^{22}Ne

TABLE 2

Adopted γ-ray energies

Source parent (daughter)	Adopted γ-energies $E_{\gamma 0}$ (keV)		
^{22}Na(^{22}Ne)	1274.53 $\pm$0.03		
^{24}Na(^{24}Mg)	1368.53 $\pm$0.05	2754.03 $\pm$0.15	
^{46}Sc(^{46}Ti)	889.25 $\pm$0.03	1120.51 $\pm$0.03	
^{60}Co(^{60}Ni)	1173.231$\pm$0.024	1332.501$\pm$0.021	
^{88}Y(^{88}Sr)	898.02 $\pm$0.03	1836.07 $\pm$0.06	
^{207}Bi(^{207}Pb)	569.68 $\pm$0.03	1063.62 $\pm$0.03	1770.14$\pm$0.08
ThC″(^{208}Pb)	583.17 $\pm$0.02	2614.58 $\pm$0.10	
^{20}F(^{20}Ne)	1633.59 $\pm$0.10		
^{26}Al(^{26}Mg)	1808.63 $\pm$0.10		
^{28}Al(^{28}Si)	1778.82 $\pm$0.10		

and ^{24}Mg were accurately known (see table 2), those for ^{20}Ne, ^{26}Mg and ^{28}Si were remeasured in order to obtain more reliable values.

^{20}Ne: Using a ^{20}F source produced in the ^{19}F(d, p)^{20}F reaction the energy of the γ-ray from the decay of the first-excited state of ^{20}Ne was measured to be $E_{\gamma 0} = 1633.58 \pm 0.10$ keV. This value is in agreement with the value $E_{\gamma 0} = 1633.7 \pm 0.3$ keV obtained by Spilling *et al.* [35]).

^{26}Mg: A recent energy measurement [36]) using a ^{26}Al source resulted in $E_{\gamma 0}$ (^{26}Mg(2$^+$))$-E_{\gamma 0}$(^{207}Bi, 1.7) $= 38.51 \pm 0.04$ keV or $E_{\gamma 0} = 1808.65 \pm 0.10$ keV, while from thermal n-capture in ^{25}Mg the energy of the de-excitation γ-ray of ^{26}Mg(2$^+$) was known to be $E_{\gamma 0} = 1808.7 \pm 0.5$ keV [ref. [37])]. Furthermore the energy difference $E_{\gamma 0}$(^{26}Mg(2$^+$))$-E_{\gamma 0}$(^{28}Si(2$^+$)) was determined to be 29.68 ± 0.15 keV from activity

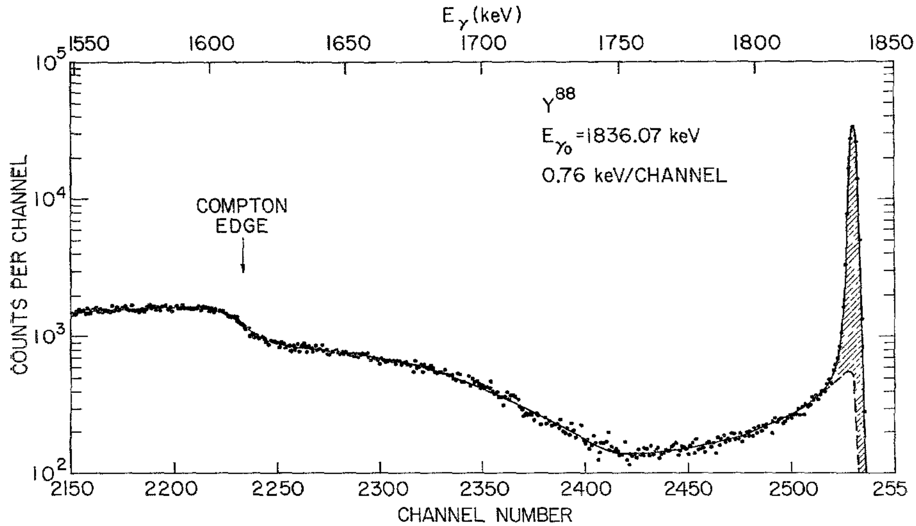

Fig. 7. Gamma lineshape for the monoenergetic 1836 keV ^{88}Y line observed in a 30 cm^3 coaxial Ge(Li) detector. The solid curve represents the best fit obtained as described in appendix B.

spectra recorded after the bombardment of ^{13}C with ^{18}O ions [38]), where both lines were observed simultaneously.

^{28}Si: A ^{28}Mg-^{28}Al source was used to remeasure the energy of the γ-rays emitted in the decay of the first excited 2^+ state of ^{28}Si. The source was prepared using the $^{26}Mg(t, p)^{28}Mg$ reaction. We obtained $E_{\gamma 0}(^{28}Si(2^+)) - E_{\gamma 0}(^{207}Bi, 1.7) = 8.72 \pm 0.03$ keV, which results in $E_{\gamma 0} = 1778.86 \pm 0.11$ keV as compared to $E_{\gamma 0} = 1778.70 \pm 0.17$ keV obtained by White *et al.* [39]). The adopted γ-energies for ^{20}Ne, ^{26}Mg and ^{28}Si are given in the lower part of table 2.

(iv) For each Ge(Li) detector used, the intrinsic lineshape of the detector, its relative photopeak efficiency, and its differential efficiency were measured in the same geom-

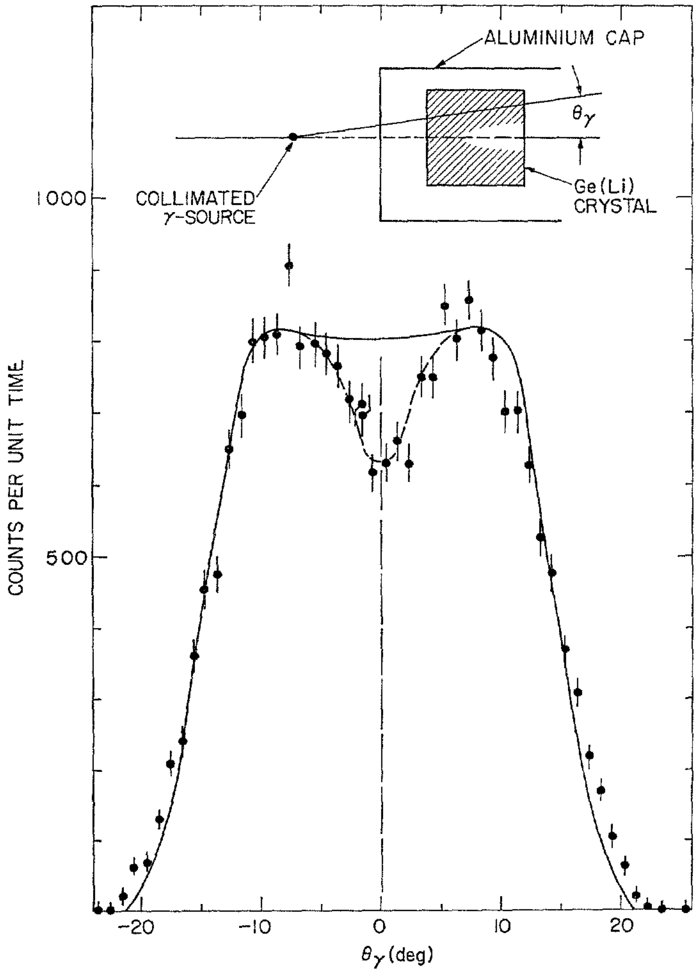

Fig. 8. Measured differential efficiency of a 45 cm^3 coaxial Ge(Li) detector for 661 keV γ-rays. The collimated γ-ray beam had a diameter of 2 mm. The distance between the source and the front face of the crystal was 5.5 cm. The solid and dashed curves are discussed in the text.

etry as in the experiment. Only coaxial detectors were used. Fig. 7 shows as an example the intrinsic γ-lineshape for 1836 keV γ-rays in a 30 cm^3 detector. The solid line represents the best fit obtained over the region $E_{\gamma 0}$ to $E_{\gamma 0} - 500$ keV using an analytic function. The function and the dependence of its parameters on $E_{\gamma 0}$ are discussed in appendix B. The relative photopeak efficiency ε_{ph} was determined in a standard way. The photopeak area was defined as discussed in appendix B and shown in fig. 7 by the shadowed area. For all detectors studied (25–45 cm^3) the photopeak efficiency for γ-ray energies between 0.7 and 2.0 MeV could be well described by $\varepsilon_{\text{ph}} \propto E_{\gamma 0}{}^{-k}$ with k of the order of 1.

The differential efficiency $\varepsilon(\theta_\gamma)$, which defines the detector efficiency as a function of angle of the incident γ-ray, was measured using a collimated γ-source of 0.6 or 1.2 MeV γ-rays. Fig. 8 shows the result for a 45 cm^3, five-sided detector obtained with 0.66 MeV γ-rays. The solid curve results from a calculation which assumed that the differential efficiency is proportional to the length of the path in the crystal; the dimensions of the crystal were obtained by scanning the detector with a γ-source. The dip of the differential efficiency at $\theta_\gamma = 0°$ is due to the fact that the central core is only partially depleted and was accounted for by subtracting a Gaussian function from the solid curve, as shown by the dashed curve in fig. 8. The dependence of the form of $\varepsilon(\theta_\gamma)$ on the γ-ray energy was found to be small for $E_{\gamma 0} > 0.6$ MeV and could be neglected for our purposes.

4. Experiments and analysis

4.1. THE STATIC QUADRUPOLE MOMENT OF ^{26}Mg(2^+)

Three measurements were performed to determine the static quadrupole moment of the first excited $I^\pi = 2^+$ state of ^{26}Mg at 1.809 MeV using a ^{37}Cl beam and targets of 200, 240 and 260 $\mu g/cm^2$. The targets were made from 99.4 % enriched ^{26}Mg and were either self-supporting or evaporated onto a 110 $\mu g/cm^2$ thick Ni foil. The initial energy of the ^{37}Cl projectiles was $E_p = 54.0$ MeV, which was reduced to $E_p = 52.65 \pm 0.03$ MeV after the ions passed through the Ni foil of the backed targets. These energies correspond to a minimum surface distance of $d = 3.1$ fm and $d = 3.5$ fm, respectively, and thus fulfill the safety requirement of subsect. 2.5.

The data shown in fig. 6a were chosen to illustrate various steps in the analysis of the ^{26}Mg experiment as well as that of the other reorientation measurements presented in this paper. Fig. 9 shows the corresponding spectrum after subtracting the background. This spectrum was obtained by subtracting in a first step the room background (fig. 6b), which was smoothed and normalized according to the intensity of the 2.6 MeV ThC″ line. Furthermore, we considered contributions from the decay of the first excited $I^\pi = \frac{1}{2}^+$ state of ^{37}Cl at 1.727 MeV, which is weakly excited in projectile collisions with the ^{26}Mg target nuclei. The γ-lineshape and relative intensity for the ^{37}Cl($\frac{1}{2}^+$) γ-ray were calculated using the measured [23]) B(E2) values for ^{37}Cl($\frac{1}{2}^+$) and ^{26}Mg(2^+). Contributions from this source amount to $\approx$ 10 counts per channel at $E_\gamma \approx 1800$ keV and are zero for energies above 1810 keV, and have been subtracted. The remaining background (approximately 20 %) was described by a straight line, which was fitted to the spectrum below and above the ^{26}Mg line taking into account the low-energy tail of the γ-ray line.

The theoretical γ-lineshape for a given quadrupole moment $Q(2^+)$ was calculated by means of a computer code, which evaluates eq. (A. 36) of appendix A including the deorientation effect as discussed in subsect. 2.6. The statistical tensors α were computed for eighteen scattering angles Θ_1 and several projectile energies using the

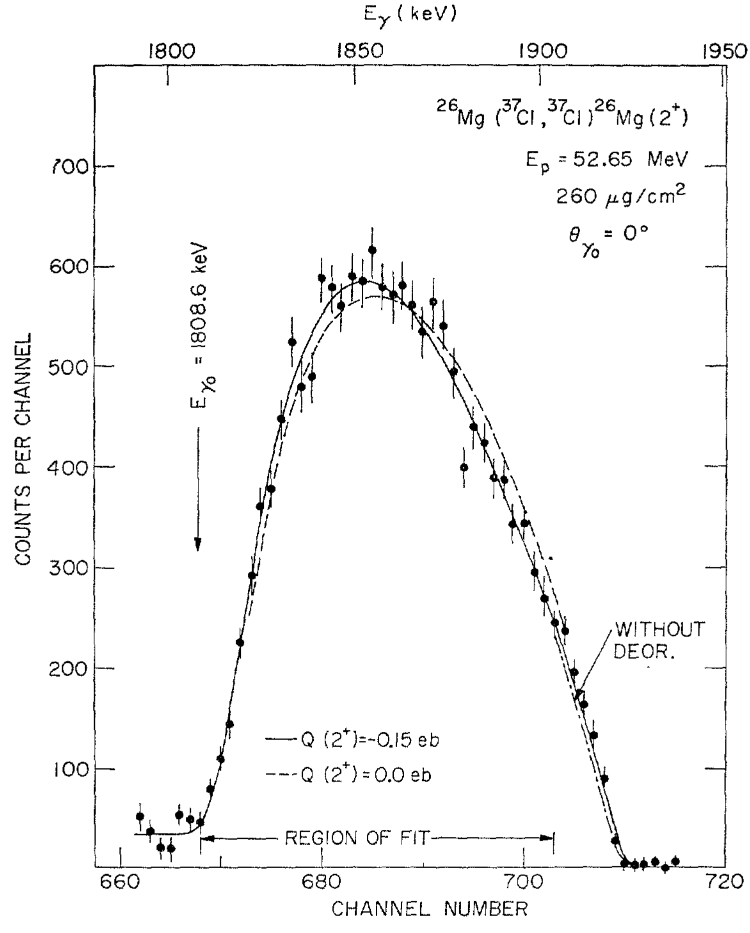

Fig. 9. The 1809 keV line of ^{26}Mg as obtained from the measurement shown in fig. 6 after subtracting the background; E_p is the energy of the ^{37}Cl projectiles after passing through the Ni foil. The solid curve illustrates the theoretical lineshape for $Q(2^+) = -0.15\ e \cdot b$ (best fit, statistical error ± 0.04 $e \cdot b$). For comparison, the best fit obtained when the effect of the deorientation is neglected ($Q(2^+) = -0.14\ e \cdot b$) is shown as well as the theoretical lineshape for $Q(2^+) = 0$. All lineshapes were calculated assuming a negative sign for $M_{12}M_{13}M_{23}$. The quoted quadrupole moments are corrected for the quantal effect.

program of Winther-de Boer [10]). The accuracy of the various interpolation routines used to calculate the γ-lineshape was studied. From these investigations the average numerical error of the calculated γ-lineshape was found to be less than 0.2 % over the full spectrum, and less than 1 % at the extreme energies. In a final step the theoretical lineshape was folded with the intrinsic lineshape of the Ge(Li) detector, taking into account the energy dependence of the photopeak efficiency.

The measured γ-ray line was then fitted with the theoretical lineshape by means of a least-squares program, the only free parameters being the quadrupole moment $Q(2^+)$ and the intensity normalization. In this program the theoretical γ-lineshape is interpolated linearly between those calculated for $Q(2^+) = 0$ and $Q(2^+) = Q_{\mathrm{rot}}$, where $Q_{\mathrm{rot}} = \frac{2}{7}[16\pi/5B(\mathrm{E2}, 0 \rightarrow 2)]^{\frac{1}{2}}$ is the value expected in the rotational model. To test this procedure, which is suggested by the perturbation approach (see eq. (1)), the fit was repeated using the lineshape for $Q(2^+) = 0$ and that calculated for the value of $Q(2^+)$ obtained in the best previous fit; deviations in the resultant best values for $Q(2^+)$ were always < 2 %. Finally the value obtained for the quadrupole moment was corrected for the quantal effects by means of table 1.

The parameters used to calculate the γ-lineshape for the measurement shown in fig. 9 are listed in table 3. In these calculations virtual excitations through the second excited 2^+ state of ^{26}Mg at 2.938 MeV were taken into account explicitly (the excitation probability of the second excited state itself is negligibly small). The size of the relevant matrix elements were taken from the literature [23, 40, 41]). The contribution

TABLE 3

Influence of the uncertainty ΔX of various input parameters X on the value of the extracted quadrupole moment for the ^{26}Mg measurement shown in fig. 9

Parameter	X	ΔX	ΔQ ($e \cdot$ b)
$\lvert M_{12}\rvert$ [a])	0.172 $e \cdot$ b	± 0.009	∓ 0.0015
$\lvert M_{13}\rvert$ [a])	0.047 $e \cdot$ b	± 0.004	0.006 [b])
$\lvert M_{23}\rvert$ [a])	0.182 $e \cdot$ b	± 0.046	
E_{p}	52.65 MeV	± 0.03	∓ 0.0013
δE_{p}	4.83 MeV	± 0.08	± 0.0012
$E_{\gamma 0} - E_{\gamma}(^{207}\mathrm{Bi}, 1.7)$	38.51 keV	± 0.05	∓ 0.008 [c])
calibration	2.7263 keV/ch	± 0.0008	± 0.002
$\cos \theta_{\gamma 0}$	1.0	-0.0014	< 0.001
efficiency constant k	1.015	± 0.030	0
target thickness	260 μg/cm^2	± 30	
dE/dx (^{26}Mg in ^{26}Mg)		± 10 %	± 0.006
τ	0.70 psec	± 0.08	
deorientation	with	without	$+0.009$
E1 polarization	without	with	$+0.006$

[a]) $M_{\mathrm{fi}} = \langle I_{\mathrm{i}} \| i^2 M(\mathrm{E2}) \| I_{\mathrm{f}} \rangle$ [see ref. [10])].

[b]) The sign of the error depends on the sign of the product $M_{12}M_{13}M_{23}$.

[c]) The error is partially due to the uncertainty in the determination of the position of the reference line.

of this effect, however, depends also on the sign of the product of the reduced E2 matrix elements, $M_{12}M_{13}M_{23}$, which is not known experimentally. Therefore the analysis was carried out for both possible signs.

The solid line in fig. 9 shows the best fit obtained for $Q(2^+) = -0.15\ e \cdot \mathrm{b}$ assuming $M_{12}M_{13}M_{23} < 0$. For $M_{12}M_{13}M_{23} > 0$ an equally good fit is obtained for $Q(2^+) = -0.12\ e \cdot \mathrm{b}$. The statistical errors, which were determined according to ref. [42]), are $\pm 0.04\ e \cdot \mathrm{b}$ in both cases. The region of fit was restricted as indicated in fig. 9 in order to minimize the possible influence of the deorientation correction on the analysis. The dash-dotted curve in fig. 9 represents the best fit if the deorientation effect is neglected. Although inside the fitting region the distortion of the γ-lineshape due to deorientation is small, agreement between the calculated and measured lineshape at high γ-energies is noticeably improved if the attenuation is included. The systematic errors in $Q(2^+)$ introduced by uncertainties in the input parameters were investigated and are listed in column 4 of table 3.

The results of our measurements for the static quadrupole moment of $^{26}\mathrm{Mg}(2^+)$ are given in table 4 together with the mean values derived for both sign assumptions. The mean values are:

$$Q(2^+) = -0.16 \pm 0.04\ e \cdot \mathrm{b}, \qquad M_{12}M_{13}M_{23} < 0,$$

$$Q(2^+) = -0.12 \pm 0.04\ e \cdot \mathrm{b}, \qquad M_{12}M_{13}M_{23} > 0.$$

TABLE 4

Summary of the experimental results

Target	$\Delta E(2^+)$ (MeV)	Projectile	E_p (MeV)	Target thickness	$Q(2^+)$ $(e \cdot \mathrm{b})$ a)	Mean value b) $Q(2^+)$ $(e \cdot \mathrm{b})$
^{20}Ne	1.634	^{32}S	41.3	10mm, 650 Torr	-0.21 ± 0.05	-0.23 ± 0.08
			40.6	5mm, 640 Torr	-0.26 ± 0.07	
^{22}Ne	1.275	^{32}S	40.6	17mm, 95 Torr	-0.16 ± 0.07	-0.18 ± 0.04
			41.3	11mm, 310 Torr	-0.22 ± 0.07	
			41.3	10mm, 300 Torr	-0.18 ± 0.04	
			41.0	5mm, 650 Torr	-0.17 ± 0.06	
^{24}Mg	1.369	^{32}S	42.0	310 μg/cm^2	-0.23 ± 0.08	-0.24 ± 0.06
			48.0	150 μg/cm^2	-0.24 ± 0.04	
			55.6	76 μg/cm^2	-0.21 ± 0.03	
			55.6	550 μg/cm^2	-0.24 ± 0.02	
^{26}Mg c)	1.809	^{37}Cl	54.00	200 μg/cm^2	-0.16 ± 0.04 (-0.13 ± 0.04)	-0.16 ± 0.04 (-0.12 ± 0.04)
			52.65	240 μg/cm^2	-0.16 ± 0.04 (-0.12 ± 0.04)	
			52.65	260 μg/cm^2	-0.15 ± 0.04 (-0.12 ± 0.04)	
^{28}Si	1.779	^{34}S	54.0	140 μg/cm^2	$+0.17 \pm 0.07$	$+0.17 \pm 0.05$
				140 μg/cm^2	$+0.19 \pm 0.07$	
				250 μg/cm^2	$+0.16 \pm 0.05$	

The quadrupole moments are corrected for the quantal effect.

a) Only statistical errors are given.

b) All known sources of error included.

c) The values enclosed in parenthesis are for $M_{12}M_{13}M_{23} > 0$, those without are for $M_{12}M_{13}M_{23} < 0$.

A negative sign of $M_{12}M_{13}M_{23}$ is predicted in the anharmonic vibrational as well as in the symmetric and asymmetric rotational model (see also discussion).

The uncertainties attached to the mean values include the systematic errors listed in table 3. The uncertainty due to the deorientation correction, which was calculated using $g = 0.5$ for the magnetic moment of the first excited state of ^{26}Mg, was estimated to be ± 0.005 $e \cdot$ b, while the possible effect of the virtual E1 excitation was considered as an additional error, $\Delta Q(\mathrm{E1}) = 0.006$ $e \cdot$ b, according to our discussion in subsect. 2.3.

4.2. THE STATIC QUADRUPOLE MOMENT OF ^{24}Mg(2^+)

Several measurements were performed using self-supporting ^{24}Mg targets (> 99 %

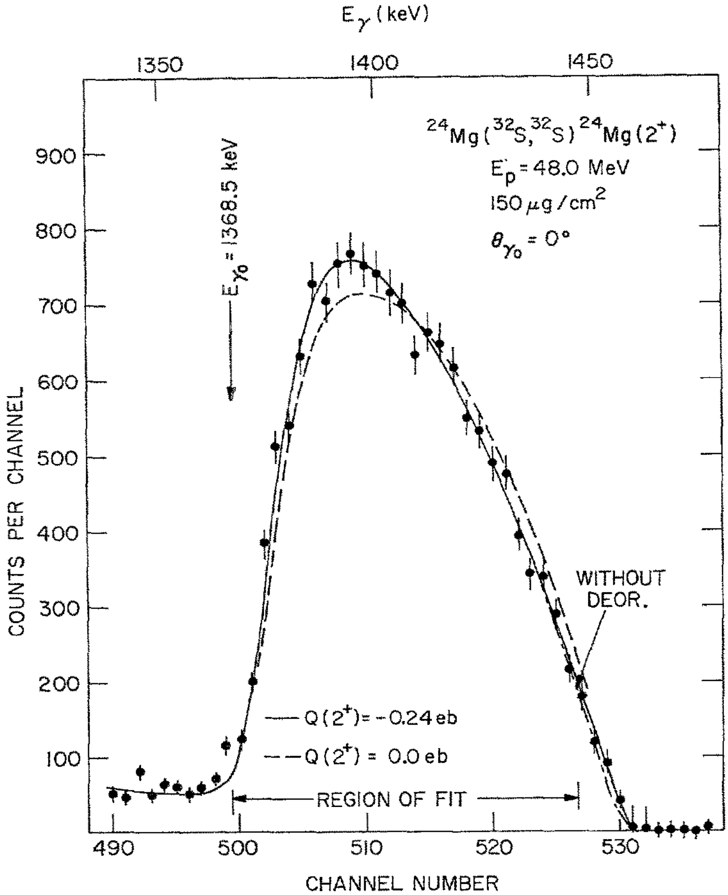

Fig. 10. The 1369 keV line of ^{24}Mg observed in the bombardment of a self-supporting ^{24}Mg target with 48 MeV ^{32}S ions. The background has been subtracted. The solid line represents the best fit obtained for $Q(2^+) = -0.24$ $e \cdot$ b. The statistical error is ± 0.04 $e \cdot$ b. For comparison, the best fit obtained when the effect of the deorientation is neglected ($Q(2^+) = -0.20$ $e \cdot$ b) is shown as well as the theoretical lineshape for $Q(2^+) = 0$ $e \cdot$ b. The quadrupole moments are corrected for the quantal effect.

enriched) with thicknesses of 76, 150, 310 and 550 $\mu g/cm^2$ and ^{32}S beams with energies between 42 MeV and 56 MeV. The 1332.5 keV line of a ^{60}Co source served as a reference line. Fig. 10 shows the relevant part of the γ-ray spectrum resulting from bombardment of the 150 $\mu g/cm^2$ target with 48.0 MeV ^{32}S ions. The background has been subtracted. The solid line represents the best fit obtained for $Q(2^+) = -0.24$ $e \cdot b$ with a statistical error of ± 0.04 $e \cdot b$. The deorientation effect was calculated assuming $g = 0.5$; the lifetime of the first excited state of ^{24}Mg was taken to be $\tau = 2.00 \pm 0.10$ psec [refs. [4, 6, 23, 43, 44])]. The measured [4, 9]) attenuation factors ($\Delta G_4 = 0.03 \pm 0.04$, $\approx 0.20 \pm 0.11$, 0.20 ± 0.07, $\approx 0.28 \pm 0.18$ for $v = 0.021$, 0.039, 0.051 and 0.061, respectively) seem to deviate somewhat systematically from the calculated ones (compare to fig. 4a). Therefore another fit was carried out in which the deorientation effect was calculated using a smooth curve through the measured attenuation coefficients. The result was $Q(2^+) = -0.23$ $e \cdot b$ as compared to -0.24 $e \cdot b$ from the previous fit, while $Q(2^+) = -0.20$ $e \cdot b$ was obtained when the deorientation effect was neglected (dashed-dotted curve in fig. 10). Similar differences of 0.03–0.04 $e \cdot b$ in the value of $Q(2^+)$ were found for all ^{24}Mg measurements when the analysis was performed with and without deorientation. The accuracy of the deorientation correction is assumed to be $\Delta Q = \pm 0.015$ $e \cdot b$.

The error in $Q(2^+)$ due to uncertainties in the calculation of the slowing-down process of the excited nuclei is $\Delta Q = \pm 0.012$ $e \cdot b$. This error comes from uncertainties in the target thickness and the stopping power function for ^{24}Mg in ^{24}Mg, and does not depend on the exact value of the nuclear lifetime, since $\gtrsim 95\,\%$ of the excited nuclei decay after emerging from the target.

The results of our measurements performed at projectile energies of 42, 48 and 55.6 MeV are listed in table 4. The values obtained at 55.6 MeV were not included in the evaluation of the mean quadrupole moment because the corresponding minimum surface distance of $d = 1.9$ fm (compared to $d = 5.7$ fm at 42 MeV and $d = 3.7$ fm at 48 MeV bombarding energy) is not safe according to our criterion. This is true even if we take into account that for the 55.6 MeV measurements our region of fit corresponds to projectile scattering angles of $\Theta_1 \lesssim 140°$, i.e. $d \geqq 2.5$ fm. However, the good agreement of the extracted quadrupole moment with those obtained at lower projectile energies supports the confidence we place in our safety requirement.

The mean value for the static quadrupole moment of the $I^\pi = 2^+$ state of ^{24}Mg at 1.369 MeV is

$$Q(2^+) = -0.24 \pm 0.06\ e \cdot b,$$

where all known sources of error are included.

4.3. THE STATIC QUADRUPOLE MOMENT OF $^{28}Si(2^+)$

The lowest $I^\pi = 2^+$ state of ^{28}Si at 1.779 MeV was excited by ^{34}S ions accelerated to 54.0 MeV ($d \geqq 3.2$ fm). The ^{34}S beam was preferred, rather than the more easily obtainable ^{32}S, ^{35}Cl and ^{37}Cl beams, because ^{34}S does not cause any background lines in the region of interest. The self-supporting targets which were used were made from natural Si(92 % ^{28}Si), in thicknesses of 140 and 250 μg/cm^2. The thicker of these was actually composed of two layers of 120 and 130 μg/cm^2 mounted 1 mm apart. The 1.770 MeV γ-rays from a ^{207}Bi source were used in all measurements to obtain a reference line. Using the measured energy difference of $E_{\gamma 0}-E_\gamma(^{207}\text{Bi}, 1.7) = 8.72\pm0.03$ keV (see sect. 3), the position of the unshifted ^{28}Si line could be determined very accurately.

In fig. 11 the γ-spectrum accumulated during the bombardment of the 250 μg/cm^2

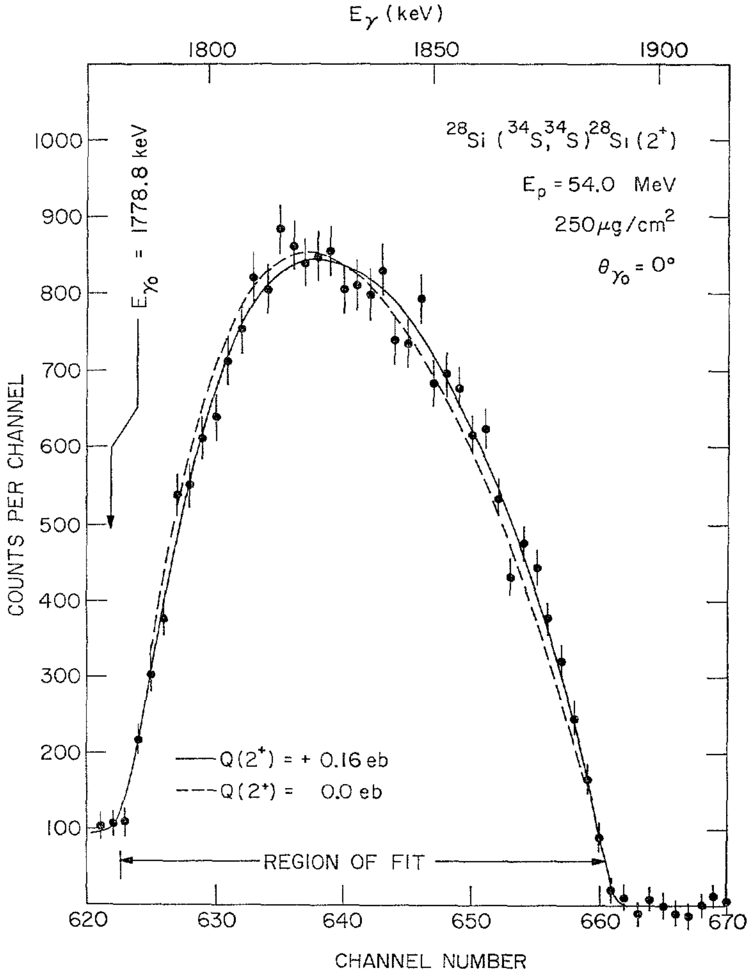

Fig. 11. The 1779 keV line of ^{28}Si observed in the bombardment of a selfsupporting ^{28}Si target with 54 MeV ^{34}S ions. The background has been subtracted. The solid line represents the best fit obtained for $Q(2^+) = +0.16\ e\cdot\text{b}$. The statistical error is $\pm0.05\ e\cdot\text{b}$. The theoretical lineshape for $Q(2^+) = 0$ is shown for comparison. The quadrupole moments are corrected for the quantal effect.

target is shown after subtraction of the background. The solid curve shows the best fit obtained for $Q(2^+) = +0.16\ e \cdot \mathrm{b}$ with a statistical error of $\pm 0.05\ e \cdot \mathrm{b}$. The γ-lineshape was calculated for both layers of the target separately using a value of $\tau = 0.72 \pm 0.05$ psec for the lifetime of $^{28}\mathrm{Si}(2^+)$ [refs. [4, 5, 45]]. The value used for the magnetic moment corresponds to $g = 0.5$.

The results obtained from the individual measurements are given in table 4. The mean value, including all systematic errors, is

$$Q(2^+) = +0.17 \pm 0.05\ e \cdot \mathrm{b}.$$

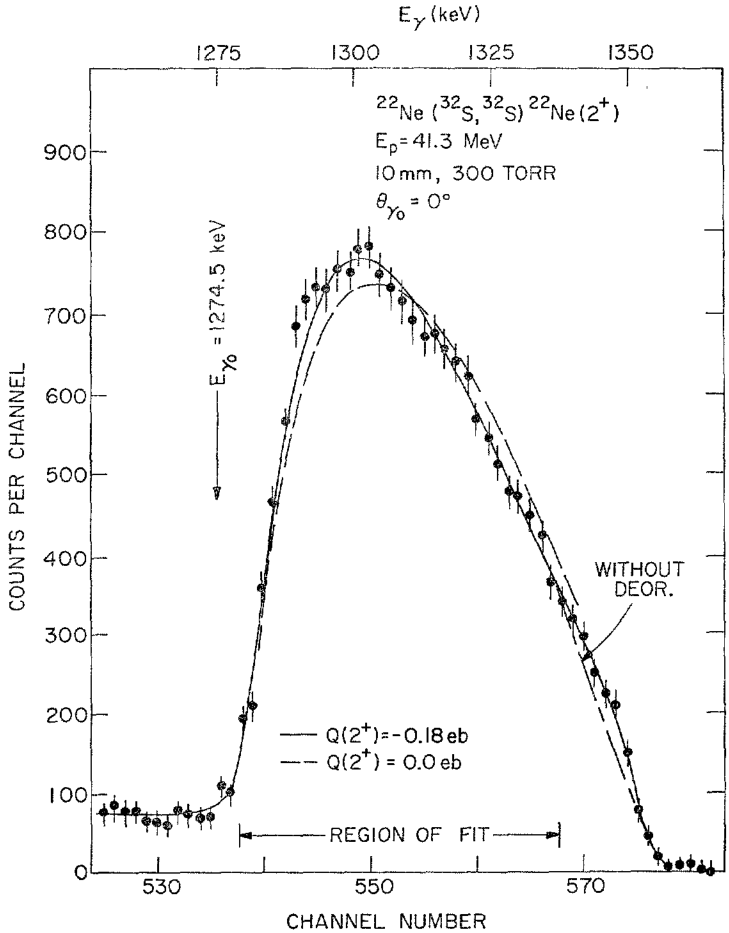

Fig. 12. The 1275 keV line of ^{22}Ne observed in the bombardment of a ^{22}Ne gas target with ^{32}S ions. The background spectrum has been subtracted; E_p is the energy of the projectiles after passing through the Ni window of the gas target. The solid line represents the best fit obtained for $Q(2^+) = -0.18\ e \cdot \mathrm{b}$ (statistical error $\pm 0.04\ e \cdot \mathrm{b}$) after correcting for the quantal effect. For comparison, the best fit obtained when neglecting the deorientation effect is shown as well as the theoretical lineshape for $Q(2^+) = 0\ e \cdot \mathrm{b}$.

4.4. THE STATIC QUADRUPOLE MOMENT OF ^{22}Ne(2$^+$)

These measurements were performed using a gas target with thicknesses between 5–17 mm and gas pressures between $p = 95$ and $p = 650$ Torr. The target was filled with neon enriched to 99 % ^{22}Ne. The effective target thickness was kept in the order of 200 to 400 μg/cm^2. A ^{32}S beam of 48 MeV was used, which was slowed down to $E_p \approx 41$ MeV by the entrance window of the gas target. This energy corresponds to a minimum surface distance of $d \approx 4$ fm and is thus well below the safe energy. The beam current was 50–100 μA (charge state 7$^+$).

In fig. 12 the relevant portion of the γ-spectrum observed with a 10 mm thick target and a gas pressure of $p = 300$ Torr is shown. The projectile energy was $E_p = 41.3 \pm 0.8$ MeV; the large error is mainly due to carbon build up on the entrance window, of 10–20 μg/cm^2, as estimated from the energy loss of 6 and 9 MeV α-particles measured before and after the experiment. The energy loss of the beam in the target was estimated as discussed in sect. 3 to be $\delta E_p = 5.0 \pm 1.5$ MeV. The background spectrum, which has been subtracted from the spectrum shown in fig. 12, was measured in a separate run where the neon gas was replaced by hydrogen but with all other conditions unchanged. The peak-to-background ratio was 10 : 1. The 1120.5 keV line of a ^{46}Sc source was used as a reference line.

The theoretical γ-lineshapes were calculated using a B(E2, 0 $\rightarrow$ 2) value of $0.020 \pm 0.002\ e^2 \cdot b^2$, which corresponds to a lifetime of $\tau = 6.0 \pm 0.6$ psec. This B(E2) value,

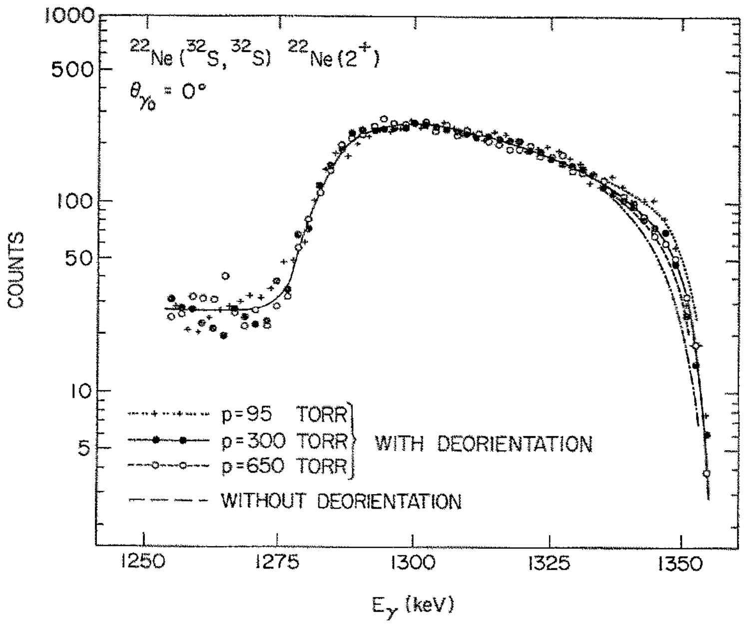

Fig. 13. Pressure dependence of the deorientation effect for ^{22}Ne(2$^+$) recoiling into a ^{22}Ne gas. The spectra were obtained in the bombardment of a ^{22}Ne gas target at different gas pressures with ^{32}S ions (see also table 4) and were normalized to the measurement at $p = 95$ Torr. The theoretical curves were calculated as described in the text.

which is the average of five lifetime measurements utilizing the recoil distance [30, 46] and Doppler shift attenuation methods [47]), is smaller than those obtained from Coulomb excitation measurements of ^{22}Ne projectiles ($0.039\pm0.014\ e^2\cdot b^2$ [ref. [48]]], $0.033\pm0.006\ e^2\cdot b^2$ [ref. [5]]], $0.026\pm0.002\ e^2\cdot b^2$ [ref. [7]]]). Since the exact B(E2) value is of minor importance for the analysis of our reorientation experiments, the value given above was used, which seems to us more reliable because of the consistency of the individual measurements despite the various methods applied.

The solid curve in fig. 12 represents the best fit obtained for $Q(2^+) = -0.18\ e\cdot b$, the statistical error being $\pm0.04\ e\cdot b$. The high-energy part of the lineshape, where the distortion due to deorientation is relatively larger, was exempted from the least-squares fit. The attenuation was calculated as discussed in subsect. 2.6 assuming a fluctuating hyperfine interaction; the proportionality constant α defined by eq. (21) was set equal to $\alpha = 1.5$ in order to achieve satisfactory agreement between the experimental and calculated γ-lineshapes at very high recoil velocities. For comparison the best fit obtained without deorientation is also shown; the deviation of the quadrupole moments deduced from these two fits was only 3 %.

A comparison of the measurements performed at $p = 95$, 300 and 650 Torr is shown in fig. 13 together with the calculated γ-lineshapes assuming $\alpha = 1.5$. Although the measurements are not decisive, the predicted dependence of the deorientation correction on the gas pressure is consistent with the experiments.

The results of the individual measurements are listed in table 4. No systematic dependence of the deduced quadrupole moments on the gas pressure is observed. The sensitivity of the extracted quadrupole moments to E_p and δE_p was studied. The attached uncertainties cause an error of $\Delta Q = \pm0.016\ e\cdot b$. All other systematic errors, including those due to the deorientation correction (3 %), the position of the unshifted ^{22}Ne line (3 %) and the E1 contribution (3 %) are much smaller, while the slowing down of the excited nuclei in the gas is negligible. The mean value for the static quadrupole moment of the 1.275 MeV state of ^{22}Ne is found to be

$$Q(2^+) = -0.18\pm0.04\ e\cdot b.$$

4.5. THE STATIC QUADRUPOLE MOMENT OF ^{20}Ne(2^+)

The reorientation measurements on the first excited state of ^{20}Ne at 1.634 MeV were carried out in the same way as those for ^{22}Ne(2^+) but using the natural mixture of Ne isotopes as the target gas (91 % ^{20}Ne). The spectrum obtained in the bombardment of a 10 mm thick target with ^{32}S ions is shown in fig. 14 after subtraction of the background. The energy of the ^{32}S ions after passing through the Ni window was 41.3 ± 0.8 MeV, which corresponds to a safe surface distance of $d = 5.1$ fm. The energy loss of the beam in the target ($p = 650$ Torr) was $\delta E_p = 10.5\pm3.0$ MeV. The influence of the uncertainty in δE_p on the quadrupole measurement is small, because the excitation probability at 31 MeV amounts to only 3 % of that at 41 MeV.

The best fit of the data shown in fig. 14 was obtained for $Q(2^+) = -0.21\ e\cdot b$.

The fit was limited to γ-energies below 1725 keV because of the somewhat uncertain subtraction of the 2754.0 keV double-escape line of a ^{24}Na source, which served as the reference line. Neither the slowing down of the excited nuclei nor the deorientation effect was considered in the analysis. These effects are much smaller here than in the ^{22}Ne measurement because of the shorter lifetime of the first excited state of ^{20}Ne: $\tau = 1.20 \pm 0.15$ psec. This value, taken as an average of several Doppler-shift attenuation measurements [49]) corresponds to $B(\mathrm{E2}, 0 \rightarrow 2) = 0.029 \pm 0.004\ e^2 \cdot \mathrm{b}^2$.

The quadrupole moments extracted from our measurements are listed in table 4. The mean value, including all sources of error, is

$$Q(2^+) = -0.23 \pm 0.08\ e \cdot \mathrm{b}.$$

Since the natural Ne gas contains 8.8 % ^{22}Ne, the ^{22}Ne line was also observed with comparable intensity because of the larger excitation probability for ^{22}Ne(2$^+$). The

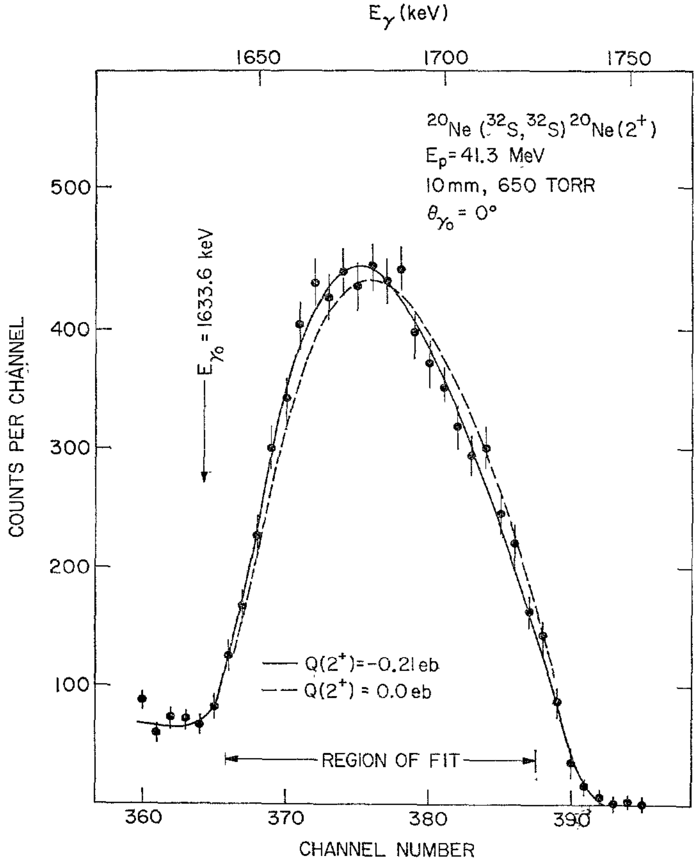

Fig. 14. The 1634 keV line of ^{20}Ne observed in the bombardment of a neon gas target with ^{32}S ions. The background spectrum has been subtracted; E_p is the energy of the projectiles after passing through the Ni window of the gas target. The solid line represents the best fit obtained for $Q(2^+) = -0.21$ $e \cdot$ b (statistical error ± 0.05) after correcting for quantal effects. For comparison, the theoretical lineshape for $Q(2^+) = 0\ e \cdot$ b is also shown. The deorientation effect is negligible.

analysis of the ^{22}Ne line, although less accurate in this case because of the larger background, results in a mean value of $Q(2^+) = -0.19\ e \cdot \mathrm{b}$ with a statistical error of $\pm 0.05\ e \cdot \mathrm{b}$, in good agreement with the results of 4.4. Furthermore the ratio of the B(E2) values for ^{20}Ne and ^{22}Ne could be extracted. Using the adopted value for ^{22}Ne of $B(\mathrm{E2}, 0 \rightarrow 2) = 0.020 \pm 0.002\ e^2 \cdot \mathrm{b}^2$, we obtain $B(\mathrm{E2}, 0 \rightarrow 2) = 0.0285 \pm 0.0043\ e^2 \cdot \mathrm{b}^2$ for ^{20}Ne, in excellent agreement with the results of the quoted lifetime measurements.

It should be pointed out that the mean value obtained from Coulomb excitation of ^{20}Ne projectiles, $B(\mathrm{E2}, 0 \rightarrow 2) = 0.039 \pm 0.003\ e^2 \cdot \mathrm{b}^2$ [refs. [4, 7, 48])], is again considerably larger than the value obtained from lifetime measurements, a discrepancy also observed in the corresponding B(E2) values for ^{22}Ne. The ratio of the average B(E2) values for ^{20}Ne-^{22}Ne obtained from the projectile excitation experiments, however, agrees with the result of our relative measurement.

5. Discussion

Our experience with the Doppler-shift method for measuring the reorientation effect in light nuclei indicates that the systematic errors inherent in this method can be kept smaller than 10–15 %; in all cases the uncertainties in the extracted static quadrupole moments were determined mainly by the statistical errors ($\approx$ 20 %). The main advantage of the Doppler-shift technique, aside from its experimental simplicity, is that it allows the simultaneous measurement of the reorientation effect for *all* scattering angles of the projectile between $0° \leqq \Theta_1 \leqq 180°$, which permits an approximate separation of the reorientation and deorientation effects according to their different dynamic behaviors. The weakest point of this method results from its sensitivity to background lines, since only singles γ-spectra are recorded. Thus a very careful study of the background and possible background sources is necessary. The technique is especially suitable for light nuclei, although its applicability to heavier nuclei is limited only by the available heavy ion beams.

The results of our measurements of the static quadrupole moments $Q(2^+)$ are listed in table 5 together with those obtained from other reorientation experiments. The absolute values for ^{20}Ne, ^{22}Ne and ^{24}Mg given in our previous publications [3]) are slightly larger and less accurate than those given in table 5 because the quantal effects were not considered explicitly but were absorbed into the quoted errors. Furthermore, in the case of ^{20}Ne our more precise measurement of the excitation energy of the first excited state has allowed a more refined analysis of the experimental data.

The largest correction to our results derives from the fact that our analysis is based on a semiclassical treatment of the Coulomb excitation process. Although the Sommerfeld parameter η is of the order of 23–30, the quantal correction still amounts to 10–15 %. These corrections should therefore be evaluated even in cases with $\eta > 30$, since they vanish only slowly, as η^{-1}, with increasing η. Unfortunately, for those measurements where the projectile-γ correlation is measured rather than the excitation probability, the quantal corrections cannot yet be obtained from the literature for geometries other than $\theta_\gamma = 0°$. However, for all experiments listed in the third column of table 5 (excluding that of ref. [6]), where the quantal effects were explicitly taken into account) these corrections should be either negligible or covered by the quoted errors.

As discussed earlier in this paper, possible contributions from virtual E1 excitation via the giant dipole states result in an uncertainty of only a few percent in the extracted quadrupole moments. The E1 contribution is expected to be about the same size for the measurements of refs. [4, 6]). This is also true for the experiments of Nakai *et al.* [5]) where the projectile excitation on medium and heavy nuclei was studied. From eqs. (1) and (9) we estimate that in these experiments the E1 contribution, relative to the reorientation effect, is enlarged by a factor of only 2–2.5 as compared to our measurements. This leads to an estimate of $\Delta Q(\mathrm{E1}) \approx 0.01\ e \cdot \mathrm{b}$. A more detailed calculation [ref. [50])] using the polarization description and reevaluating $Q(2^+)$ *and* $B(\mathrm{E2}, 0 \to 2)$ of ref. [5]) shows indeed, that the E1 contribution amounts to $\Delta Q(\mathrm{E1}) \leqq +0.003\ e \cdot \mathrm{b}$ for ^{20,22}Ne and $\Delta Q(\mathrm{E1}) \leqq +0.01\ e \cdot \mathrm{b}$ for ^{28}Si. Similarly for the measurements of ref. [7]), where the projectile excitation of the neon isotopes impinging on Pt and Au targets is studied and the quadrupole moments are extracted from the γ-ray angular distribution, the E1 contribution was found to be negligible. Thus, the influence of the giant dipole states on the reorientation experiments in sd shell nuclei is felt to be only of minor importance.

TABLE 5

Comparison of the present results with those obtained in other laboratories and theoretical predictions

Nucleus	Experimental results $Q(2^+)$ ($e \cdot$ b) present	others	Ref.	Theoretical predictions $Q(2^+)$ ($e \cdot$ b) RM [a]) $2 \to 0$	RM [a]) $4 \to 2$	TRM [b])	SM [c])	HF [d])
^{20}Ne	-0.23 ± 0.08	-0.24 ± 0.03	[5])	0.15	0.14		-0.14	-0.15
		-0.20 ± 0.06	[7])	± 0.01	± 0.01			
^{22}Ne	-0.18 ± 0.04	-0.21 ± 0.04	[5])	0.13	0.14		-0.14	-0.15
		-0.09 ± 0.04	[7])	± 0.01	± 0.01			
^{24}Mg	-0.24 ± 0.06	-0.24 ± 0.04	[4])	0.19	0.16	-0.15	-0.16	-0.18
		-0.38 ± 0.16	[4])	± 0.01	± 0.01			
		-0.31 ± 0.07	[6])					
		-0.19 ± 0.05	[4])					
^{26}Mg	-0.16 ± 0.04			0.16	0.09	-0.13	$+0.04$	-0.18
	(-0.12 ± 0.04)			± 0.01	± 0.03			
^{28}Si	$+0.17 \pm 0.05$	$+0.17 \pm 0.05$	[4])	0.16	0.11		$+0.16$	$+0.18$
		$+0.22 \pm 0.09$	[4])	± 0.01	± 0.01			
		$+0.11 \pm 0.05$	[5])					

[a]) Rotational model (see text). Only the absolute value of $Q(2^+)$ can be predicted in these calculations.

[b]) Triaxial rotational model [ref. [52])]. [c]) Shell model [ref. [53])].

[d]) Hartree-Fock calculations [ref. [54])].

The overall agreement of our results with those obtained in other reorientation experiments is good (see table 5), and the accuracies are comparable. The only exception occurs in ^{22}Ne, where the quadrupole moment obtained by Olsen *et al.* [7]) is considerably smaller than our value and that of ref. [5]), while the corresponding measurements for ^{20}Ne agree within the experimental errors. The reason for this discrepancy is not yet understood.

To summarize the experimental results: Large quadrupole moments are observed for the first excited 2^+ states of all stable, even-A nuclei in the beginning of the sd shell together with an abrupt sign change between ^{26}Mg and ^{28}Si. In the following we shall discuss these experimental results in terms of several theoretical models.

The static quadrupole moments $Q(2^+)$ are most commonly compared to the predictions of the axially symmetric rotational model. The values listed in columns 5 and 6 of table 5 were calculated from the E2 transition moments [given in sect. 4 and refs. [49, 51])] in the $K = 0$ ground state band using

$$Q(I) = Q_0 \frac{3K^2-I(I+1)}{(I+1)(2I+3)}, \tag{22}$$

$$Q_0^2 = \frac{16\pi}{5(2I_f+1)} \begin{pmatrix} I_i & 2 & I_f \\ K & 0 & -K \end{pmatrix}^{-2} B(\mathrm{E2}, I_i \rightarrow I_f). \tag{23}$$

The quadrupole moments $Q(2^+)$ calculated by means of eqs. (22) and (23) from different transitions within the ground state band must be constant, if the simple rotational picture is to provide an adequate description of these states. For the even-A nuclei listed in table 5, this seems to be the case only for ^{20}Ne and ^{22}Ne, although deviations from the rotational model are known to exist also for these nuclei if higher transitions in the ground state band are considered [49]). The measured static quadrupole moments of the 2^+ states of ^{20}Ne and ^{22}Ne, however, seem to be about 20–30 % larger than those predicted in this model. For ^{24}Mg, ^{26}Mg and ^{28}Si, the E2 properties of the $2 \rightarrow 0$ and $4 \rightarrow 2$ transitions do not agree with the rotational prediction. Thus the relation of the static and dynamic quadrupole moments as provided by the rotational model is not necessarily meaningful. In contrast to this the rotational model is known to work well for all odd-A nuclei in this mass region.

The corresponding comparison between static and dynamic quadrupole moments in terms of the intrinsic moments Q_0 is illustrated schematically in fig. 15 for even- and odd-A nuclei with $20 \leqq A \leqq 28$. The solid points give the intrinsic quadrupole moments deduced from B(E2) values measured for the lowest transition within the ground state band [eq. (23)]. For odd-A nuclei the crosses give the values deduced [eq. (22)] from the ground state quadrupole moments determined in atomic/molecular spectroscopy. As can be seen the agreement is remarkably good.

For even-A nuclei the open symbols in fig. 15 give the corresponding Q_0 values deduced from the static quadrupole moments $Q(2^+)$ measured in reorientation experiments. It is somewhat more difficult in these cases to assess possible systematic errors, and we therefore chose to present the individual results. While the overall agreement between the individual values and those calculated from the B(E2)'s appears reasonable, there is evidence for a systematic variance in the results for the lighter even-A nuclei.

Recently Kurath [52]) calculated the E2 properties of ^{24}Mg and ^{26}Mg using an adiabatic model of a triaxial deformed rotor. In this model, the quadrupole properties of the low-lying states are obtained from an intrinsic state with particles in the lowest-energy levels of a triaxially deformed potential well. These calculations lead back to an axially symmetric deformation for ^{24}Mg, while for ^{26}Mg a triaxial shape is obtained, which results in a reasonable description of the excitation energies and E2 transition moments in ^{26}Mg. The predicted static quadrupole moments for ^{24}Mg and ^{26}Mg are given in column 7 of table 5. The calculated value of $Q(2^+) = -0.13$ $e \cdot$ b for ^{26}Mg should be compared to the experimental value $Q(2^+) = -0.16 \pm 0.04$ $e \cdot$ b, because within this model (as in the axially symmetric rotational model), a

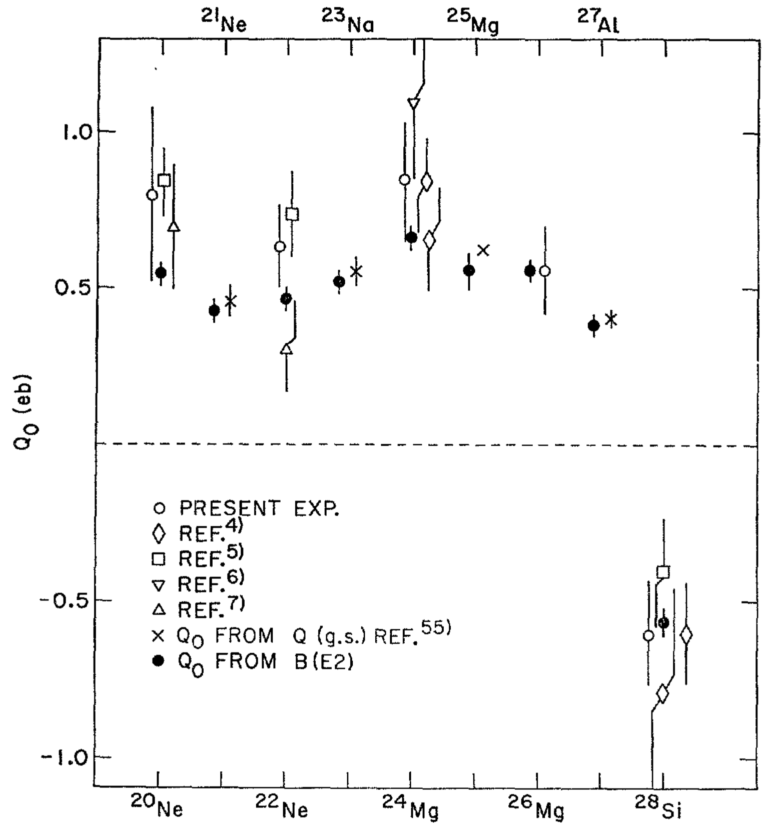

Fig. 15. Comparison of the intrinsic quadrupole moments Q_0 calculated from experimental static moments and B(E2) values in the framework of the rotational model. The B(E2) values used were those between the lowest two members of the ground state rotational band; the signs of the correspondent Q_0 values were chosen to match the observed ones.

negative sign is predicted for the product of the reduced E2 matrix elements $M_{12}M_{13}M_{23}$. A negative sign is also obtained if the E2 properties of the low-lying 2^+ states in ^{26}Mg are described in the anharmonic vibrational model, in which the one-phonon 2^+ state and the two-phonon 2^+ state are allowed to mix.

The results of recent shell-model calculations [53]) are listed in column 8 of table 5. These calculations were carried out in the full space of sd shell-model wave functions for nuclei with $A \leqq 22$, while for $A > 22$ the space was truncated in order to make the calculation feasible. Additive effective charges of 0.5 e were assumed (0.7 e for ^{25,26}Mg and ^{27}Al) for both protons and neutrons in order to obtain reasonable overall agreement between the measured and calculated E2 transition moments. While these calculations reproduce the observed ground state quadrupole moments in odd-A nuclei quite well, they underestimate those of ^{20,22}Ne and ^{24}Mg. Furthermore, a quadrupole moment of $Q(2^+) = +0.04\ e \cdot \mathrm{b}$ is predicted for ^{26}Mg in direct contradiction to experiment.

Gunye [54]) has emphasized that the truncation of the configuration space can cause an underestimation of the size of the static quadrupole moments $Q(2^+)$. His results, which were calculated from projected Hartree-Fock wave functions including the first five major oscillator shells, are compiled in the last column of table 5. Only a small additive effective charge of 0.2 e was necessary to achieve agreement with the observed E2 transition moments. While for odd-A nuclei the calculated quadrupole moments agree with those obtained in the shell-model calculations, he predicts somewhat larger quadrupole moments for even-A nuclei. In particular, $Q(2^+) = -0.18\ e \cdot \mathrm{b}$ is obtained for ^{26}Mg.

Both the shell-model and Hartree-Fock calculations, which were performed assuming constant additive effective charges, do predict the general trend of the observed static quadrupole moments $Q(2^+)$, especially the sign change between ^{24}Mg and ^{28}Si. But since the effective charge has to account for the various restrictions of the configuration space as well as for the special choice of the radial part of the wave functions and other shortcomings of the assumed model, one can question the assumption of a constant effective charge for adjacent nuclei. Note for example, that the ratios of experimental $B(\mathrm{E2}, 0 \rightarrow 2)$ values for the even neon and magnesium isotopes are quite accurately known [23]) to be 1.43 ± 0.08 for ^{20}Ne/^{22}Ne and 1.39 ± 0.07 for ^{24}Mg/^{26}Mg. These values are not reproduced in the shell-model [53]) and HF calculations [54]), which yield ratios between 0.9 and 1.0.

To avoid the difficulties connected with the proper choice of the effective charges, we calculated the ratio $|Q(2^+)|/\sqrt{B(\mathrm{E2}, 0 \rightarrow 2)}$, which is approximately independent of the effective charge for $\Delta T = 0$ transitions in light sd shell nuclei [53]), the relation being correct for self-conjugate nuclei. The experimental results are 1.35 ± 0.2, 1.15 ± 0.25, 1.15 ± 0.2, 0.90 ± 0.25 (0.7 ± 0.25) and 0.90 ± 0.2 for ^{20}Ne, ^{22}Ne, ^{24}Mg, ^{26}Mg and ^{28}Si, respectively, if average values for $Q(2^+)$ are used based on all measurements listed in table 5. The shell model predictions [53]) are 0.92, 0.84, 0.90, 0.22 and 0.93, respectively, while for the calculations of Gunye [54]) this ratio is 0.9 as in the rotational model. This comparison shows that even more refined model calculations (as provided, for example, by the shell-model) which can explain the dynamic E2 properties of the low-lying states fairly well, predict ratios of $|Q(2^+)|/\sqrt{B(\mathrm{E2}, 0 \to 2)}$ which are not significantly larger than the rotational value of 0.9. Thus they cannot explain the large observed quadrupole moments of ^{20}Ne, ^{22}Ne, and ^{24}Mg *and* the corresponding B(E2) values, regardless of the actual choice of the effective charge.

Unfortunately, in the case of the neon isotopes the quantitative comparison between the static and dynamic quadrupole moments is somewhat aggravated by inconsistencies in the measured $B(\mathrm{E2}, 0 \to 2)$ values. A decisive determination of the B(E2) values of these nuclei and also additional accurate quadrupole measurements are desirable so that a decision can be reached as to whether or not these deviations are significant and due to a yet unknown contribution to the Coulomb excitation process or a nuclear structure effect. But even in the present stage we may conclude that the reorientation measurements in sd shell nuclei add an interesting spectroscopic datum to the discussion of the structure of light nuclei.

One of us (D.S.) would like to thank the Max Kade Foundation for a generous grant given to him during the academic year 70/71. B.P. is grateful to the Brookhaven National Laboratory for an invitation as a summer visitor in 1971. A critical check of the E1 contribution to the Coulomb excitation process by Drs. K. Baur, U. Smilansky and H. Weidenmüller is gratefully acknowledged.

Appendix A

DERIVATION OF THE γ-LINESHAPE

A. 1. *Thin targets.* We first calculate the γ-lineshape assuming an infinitesimally thin target; the corrections due to the finite thickness of the target are derived in appendix A. 2. We furthermore assume, in order to simplify the following discussion, that only two levels are involved in the Coulomb excitation process, namely the $I_i^\pi = 0^+$ ground state and the $I_f^\pi = 2^+$ first excited state at an excitation energy ΔE (in MeV). To allow application of these formulae to both projectile and target excitation, the subscript j is used with the convention $j = 1$ for projectile and $j = 2$ for target excitation.

We summarize some of the relevant kinematic formulae frequently used throughout this appendix: If A_1, Z_1 and A_2, Z_2 are the mass (in amu) and charge number of the projectile and target, respectively, and E is the lab energy of the projectile (in MeV), the velocity of the c.m. is given by (all velocities are in units of the velocity of light)

$$v_{\mathrm{c.m.}} = 0.04634(1+A_2/A_1)^{-1}(E/A_1)^{\frac{1}{2}}, \tag{A.1}$$

while the velocity of the excited nucleus in the c.m. system can be written as

$$v_{sj} = v_{\mathrm{c.m.}}\kappa_j, \tag{A.2}$$

with

$$\kappa_1 = (A_2/A_1)(1-k)^{\frac{1}{2}}, \tag{A.3a}$$

$$\kappa_2 = (1-k)^{\frac{1}{2}}. \tag{A.3b}$$

The quantity k measures the inelasticity of the scattering process and is defined by

$$k = (1+A_1/A_2)\Delta E/E. \tag{A.4}$$

The velocity of the excited nucleus in the lab system is given by

$$v_j = v_{\text{c.m.}}(1+\kappa_j^2+(-1)^{j-1}2\kappa_j \cos\Theta_1)^{\frac{1}{2}}, \tag{A.5}$$

where Θ_1 is the scattering angle of the projectile in the c.m. system.

The scattering angle θ_j, φ_j of the excited nucleus in the lab system is connected with Θ_1, ϕ_1 by

$$\cos\theta_j = (v_{\text{c.m.}}/v_j)[1+(-1)^{j-1}\kappa_j \cos\Theta_1], \tag{A.6}$$

$$\varphi_1 = \phi_1, \qquad \varphi_2 = \phi_1+\pi. \tag{A.7}$$

The γ-ray lineshape is determined by the double-differential cross section for the inelastic scattering of the projectile with initial energy E into $\mathrm{d}\Omega_1$ and the subsequent emission of a γ-ray into $\mathrm{d}\Omega_\gamma$. This quantity is given by (compare with ref. [10])

$$\frac{\mathrm{d}\sigma_\gamma(\Theta_1, \Theta_\gamma, \phi_\gamma-\phi_1)}{\mathrm{d}\Omega_1\,\mathrm{d}\Omega_\gamma} = \frac{\mathrm{d}\sigma_{\mathrm{R}}(\Theta_1)}{\mathrm{d}\Omega_1}(4\pi)^{-\frac{1}{2}} \sum_{\substack{k=0,2,4\\ -k\leqq\kappa\leqq k}} \alpha_{k\kappa}(\Theta_1)F_k(2,2,0,2)Y_{k\kappa}(\Theta_\gamma, \phi_\gamma-\phi_1), \tag{A.8}$$

where the Rutherford cross section can be written as

$$\frac{d\sigma_{\mathrm{R}}(\Theta_1)}{\mathrm{d}\Omega_1} = 5.184\times10^{-3}(1-k)^{-\frac{1}{2}}\left[(1+A_1/A_2)\frac{Z_1Z_2}{E}\right]^2(1-\cos\Theta_1)^{-2}. \tag{A.9}$$

The statistical tensor $\alpha_{k\kappa}$ is connected with the excitation amplitudes via eqs. (49) and (50) of ref. [10]) (their coordinate system 3); $F_k(L, L', I_{\mathrm{f}}, I_{\mathrm{i}})$ are the usual γ-γ correlation coefficients [11]).

The γ-emission angles Θ_γ, ϕ_γ are given in a coordinate system for which the excited nucleus is at rest (fig. 16a). The transformation into the lab system is lengthy but straightforward. If θ_γ, φ_γ (or $\boldsymbol{k}_\gamma$) define the direction of the γ-ray in the lab system we obtain

$$\cos\Theta_\gamma = \frac{\cos\theta_\gamma(1-v_j^2)^{\frac{1}{2}}-\cos\theta_j v_j+\cos\theta_j\cos\theta_{\gamma j}[1-(1-v_j^2)^{\frac{1}{2}}]}{1-v_j\cos\theta_{\gamma j}}, \tag{A.10}$$

with

$$\cos\theta_{\gamma j} = \cos\theta_\gamma\cos\theta_j+(-1)^{j-1}\sin\theta_j\sin\theta_\gamma\cos(\varphi_\gamma-\phi_1), \tag{A.11}$$

$$\cos(\phi_\gamma-\phi_1) = (-1)^{j-1}\frac{\cos\theta_{\gamma j}-\cos\theta_j\cos\Theta_\gamma-v_j(1-\cos\theta_j\cos\Theta_\gamma\cos\theta_{\gamma j})}{\sin\Theta_\gamma\sin\theta_j(1-v_j\cos\theta_{\gamma j})}, \tag{A.12}$$

$$\left|\frac{\mathrm{d}\cos\Theta_\gamma\,\mathrm{d}\phi_\gamma}{\mathrm{d}\cos\theta_\gamma\,\mathrm{d}\varphi_\gamma}\right| = \frac{1-v_j^2}{(1-v_j\cos\theta_{\gamma j})^2}\,. \tag{A.13}$$

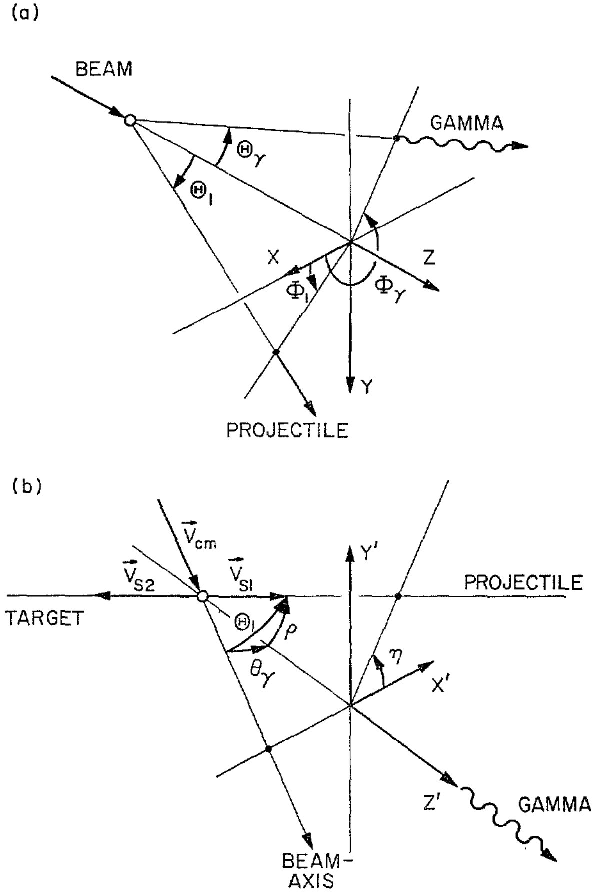

Fig. 16. a) Definition of the polar coordinates Θ_1, ϕ_1, and Θ_γ, ϕ_γ used to describe the projectile-γ correlation function (eq. (A8)). Θ_1 and ϕ_1 are the polar and azimuthal angle of the inelastic scattered projectile in the c.m. system, while Θ_γ, ϕ_γ are the corresponding angles of the emitted γ-ray in a system where the emitting nucleus is at rest. b) Definition of the c.m. coordinates ρ, η.

Here $\theta_{\gamma j}$ is the angle between $\boldsymbol{k}_\gamma$ and velocity of the excited nucleus in the lab system, $\boldsymbol{v}_j$. The energy E_γ of the de-excitation γ-rays in the lab system is given by

$$E_\gamma = E_{\gamma 0} \frac{(1-v_j^2)^{\frac{1}{2}}}{1-v_j \cos \theta_{\gamma j}}, \tag{A.14}$$

where $E_{\gamma 0}$ is the energy of the γ-ray in the rest system of the excited nucleus. In first order in v, eq. (A.14) reduces to the well-known relation $E_\gamma = E_{\gamma 0}(1+v_j \cos \theta_{\gamma j})$.

In order to derive the γ-lineshape for a given detection direction $\boldsymbol{k}_\gamma$ we must sum eq. (A.8) over all excited nuclei (i.e., over the corresponding projectiles) which contribute to the intensity at a given Doppler shift $\Delta E_\gamma = E_\gamma - E_{\gamma 0}$. The summation is carried out in a c.m. coordinate system $\boldsymbol{X'Y'Z'}$ oriented in such a way that $\boldsymbol{Z'}$ coincides with $\boldsymbol{k}_\gamma$ and X' lies in the plane defined by the beam axis and $\boldsymbol{k}_\gamma$ (fig. 16b). The polar coordinates ρ and η of $\boldsymbol{v}_{s1}$ in this coordinate system are connected with Θ_1, ϕ_1 by

$$\cos \Theta_1 = \cos \theta_\gamma \cos \rho - \sin \theta_\gamma \sin \rho \cos \eta, \tag{A.15}$$

$$\cos (\varphi_\gamma - \phi_1) = -(\cos \theta_\gamma \sin \rho \cos \eta + \sin \theta_\gamma \cos \rho)/\sin \Theta_1, \tag{A.16}$$

$$\left| \frac{\mathrm{d} \cos \Theta_1 \, \mathrm{d}\phi_1}{\mathrm{d} \cos \rho \, \mathrm{d}\eta} \right| = 1. \tag{A.17}$$

In these coordinates the projection of the velocity of the excited nucleus on the detection direction $\boldsymbol{k}_\gamma$ is given by

$$v_j \cos \theta_{\gamma j} = v_{\mathrm{c.m.}} \cos \theta_\gamma + (-1)^{j-1} v_{sj} \cos \rho, \tag{A.18}$$

which is the generalization of eq. (3) given in the main text. Thus to first order in v the Doppler shift ΔE_γ is independent of η and the integration over η would correspond to the integration over all decaying nuclei contributing to the intensity observed for a given Doppler shift ΔE_γ.

Since we are dealing with rather high recoil velocities ($v \lessapprox 0.07$) the first order approximation of ΔE_γ is normally too rough. Using the expansion

$$\Delta E_\gamma = E_{\gamma 0} \frac{v_j \cos \theta_{\gamma j} - 0.5 v_j^2}{1 - v_j \cos \theta_{\gamma j}}, \tag{A.19}$$

which is correct up to second order in v, and approximating v_j^2 by

$$v_j^2 \approx v_{\mathrm{c.m.}}^2 (1 + \kappa_j^2 + (-1)^{j-1} 2\kappa_j \cos \theta_\gamma \cos \rho), \tag{A.20}$$

which is obtained from eqs. (A.5) and (A.15) with $\cos \eta = 0$, ΔE_γ is again independent of η. The approximation leading to eq. (A.20) is good for $\kappa_j \gg 1$, i.e., projectile excitation on heavy target nuclei, or for $\sin \theta_\gamma \ll 1$, and is correct for $\theta_\gamma = 0°$.

For a given detection direction $\boldsymbol{k}_\gamma$ the γ-lineshape is then given by

$$\frac{\mathrm{d}n(\Delta E_\gamma, \theta_\gamma, \varphi_\gamma)}{\mathrm{d}\Delta E_\gamma \, \mathrm{d} \cos \theta_\gamma \, \mathrm{d}\varphi_\gamma} = (1 + \Delta E_\gamma / E_{\gamma 0})^2 \frac{\mathrm{d} \cos \rho}{\mathrm{d}\Delta E_\gamma} \times 2 \int_0^\pi \frac{\mathrm{d}\sigma_\gamma(\Theta_1(\eta), \Theta_\gamma(\eta), \phi_\gamma(\eta) - \phi_1(\eta))}{\mathrm{d}\Omega_1 \, \mathrm{d}\Omega_\gamma} \mathrm{d}\eta, \tag{A.21}$$

where only the η-dependence of the angles $\Theta_1, \phi_1, \Theta_\gamma$ and ϕ_γ is written explicitly; these angles are connected to the variables ΔE_γ, θ_γ, φ_γ, and η via the formulae given above and

$$\cos \rho = (-1)^{j-1} \frac{\Delta E_\gamma / E_{\gamma 0} - (1 + \Delta E_\gamma / E_{\gamma 0}) v_{\mathrm{c.m.}} \cos \theta_\gamma + 0.5 (v_{\mathrm{c.m.}}^2 + v_{sj}^2)}{v_{sj} (1 + \Delta E_\gamma / E_{\gamma 0} - v_{\mathrm{c.m.}} \cos \theta_\gamma)}. \tag{A.22}$$

Eq. (A.21) is valid up to second order in v with the restrictions given above. It should be noted that considering the Doppler shift up to second order in v is consistent with calculating the kinematics of the process in the non-relativistic limit; the relativistic corrections to eqs. (A.1) to (A.7) give rise to third-order terms in v in the Doppler shift.

Finally we have to integrate eq. (A.21) over the finite solid angle of the γ-detector. Since the γ-lineshape eq. (A.21) is independent of φ_γ, we obtain

$$\frac{\mathrm{d}N(\Delta E_\gamma)}{\mathrm{d}\Delta E_\gamma} = \int_{\cos\theta_{\gamma\,\mathrm{min}}}^{\cos\theta_{\gamma\,\mathrm{max}}} \frac{\mathrm{d}n(\Delta E_\gamma, \theta_\gamma, \varphi_\gamma = 0)}{\mathrm{d}\Delta E_\gamma \mathrm{d}\cos\theta_\gamma \mathrm{d}\varphi_\gamma} e(\theta_\gamma)\mathrm{d}\cos\theta_\gamma, \tag{A.23}$$

with

$$e(\theta_\gamma) = 2\int_0^{\varphi_{\mathrm{max}}} \varepsilon(\beta(\theta_\gamma, \varphi_\gamma))\mathrm{d}\varphi_\gamma. \tag{A.24}$$

Here, $\varepsilon(\beta)$ is the differential efficiency of the axially symmetric detector, β being the angle of the incident γ-ray relative to the symmetry axis of the detector. The angle β is related to θ_γ and φ_γ by

$$\cos\beta = \cos\theta_{\gamma 0}\cos\theta_\gamma + \sin\theta_{\gamma 0}\sin\theta_\gamma\cos\varphi_\gamma, \tag{A.25}$$

where $\theta_{\gamma 0}$ is the angle between the symmetry axis of the detector and the beam axis.

A. 2. *Corrections due to the finite target thickness.* The energy loss of a heavy ion beam, even in a 100 μg/cm^2 target, amounts to a few MeV. Since the Coulomb excitation cross section is strongly energy dependent, we must integrate the lineshape derived in appendix A. 1 over the target thickness. Furthermore, we have to consider effects on the γ-lineshape due to energy losses of the excited nuclei in the target. While the integration over the energy loss of the beam in the target is straightforward, the influence of the energy loss of the excited nucleus on the lineshape needs some further considerations.

To calculate the latter correction we assume that the direction of the nucleus does not change during the slowing-down process. This assumption is good because at velocities of several percent of the velocity of light nuclear collisions are very unlikely. The specific energy loss can then be written as

$$-\frac{\mathrm{d}E}{\mathrm{d}(\rho x)} = -\frac{Mc\,\mathrm{d}V}{\rho\,\mathrm{d}t} = f(V), \tag{A.26}$$

where ρ is the density of the target material and M and V are the mass and velocity of the moving ion. The specific energy loss was parameterized by

$$f(V) = k_\mathrm{n}(V_0/V) + k_\mathrm{e}(V/V_0) + k_3(V/V_0)^3, \tag{A.27a}$$

for velocities $V \lessapprox 5V_0$ ($V_0 = \frac{1}{137}$),

$$f(V) = a + b(V/V_0) + c(V/V_0)^2, \tag{A.27b}$$

for higher velocities. While k_n was taken from ref. [56]) and k_e from ref. [57]), k_3 was chosen to match the magnitude and derivative of $f(V)$ to those given by eq. (A.27b) at a suitable velocity V_{cut}. The parameters a, b and c were obtained by a least-squares fit to the energy loss calculated as described in refs. [23, 31]).

Using eq. (A.26) we obtain for the probability that an excited nucleus with initial velocity v_j decays at a velocity $V_j (v_j \geqq V_j \geqq V_{j\min})$

$$g(v_j, V_j)\mathrm{d}V_j = \frac{M_j c}{\rho f(V_j)\tau} \exp\left(-\frac{t(v_j, V_j)}{\tau}\right)\mathrm{d}V_j + \delta(V_j, V_{j\min}) \exp\left(-\frac{t(v_j, V_{j\min})}{\tau}\right), \tag{A.28}$$

where $t(v_j, V_j)$ is obtained by integrating eq. (A.26) with the initial condition $V_j = v_j$ for $t = 0$ (the mean lifetime of the excited nucleus is τ). The second term of eq. (A.28) describes that fraction of excited nuclei which escape from the target with velocity $V_{j\min}$ before their decay.

If we restrict ourselves to detection angles $\theta_\gamma \approx 0°$, the γ-lineshape for a given projectile energy E can then be calculated from the lineshape at $t = 0$, which is given by eq. (A.21), in the following way: For $\theta_\gamma = 0°$ and $t = 0$ all excited nuclei contributing to the intensity at a given Doppler shift ΔE_γ have the same initial velocity v_j. Therefore for $\sin\theta_\gamma \ll 1$ the deviation of the initial velocities v_j, contributing to a given ΔE_γ, from the average velocity $\bar{v}_j$ defined by

$$\bar{v}_j = v_{\text{c.m.}}(1+\kappa_j^2+(-1)^{j-1}2\kappa_j \cos\theta_\gamma \cos\rho)^{\frac{1}{2}}, \tag{A.29}$$

is small. Furthermore, we define a mean recoil angle by

$$\cos\bar{\theta}_j = (v_{\text{c.m.}}/\bar{v}_j)(1+(-1)^{j-1}\kappa_j \cos\theta_\gamma \cos\rho), \tag{A.30}$$

and a mean projection angle by

$$\cos\bar{\theta}_{\gamma j} = (v_{\text{c.m.}} \cos\theta_\gamma + (-1)^{j-1} v_{sj} \cos\rho)/\bar{v}_j. \tag{A.31}$$

Eqs. (A.29) to (A.31) follow from the relevant formulae given in appendix A. 1 with $\cos\eta = 0$.

The Doppler shift $\Delta E'_\gamma$ is connected with the velocity V_j of the excited nucleus at the moment of its decay by (compare to eq. (A.19))

$$\Delta E'_\gamma = E_{\gamma 0} \frac{V_j \cos\bar{\theta}_{\gamma j} - 0.5 V_j^2}{1 - V_j \cos\bar{\theta}_{\gamma j}}, \tag{A.32}$$

with $\bar{v}_j \geqq V_j \geqq V_{j\min}$. To calculate $V_{j\min}$ we define an effective target thickness D_{eff} by

$$D_{\text{eff}} = [D - R(E_{\text{p}}, E)]/\cos\bar{\theta}_j, \tag{A.33a}$$

$$D_{\text{eff}} = R(E_{\text{p}}, E)/\cos\bar{\theta}_j, \tag{A.33b}$$

for $\cos\bar{\theta}_j > 0$ and $\cos\bar{\theta}_j < 0$, respectively. Here D is the target thickness and $R(E_{\text{p}}, E)$ is the range of the projectile with initial energy E_{p} and final energy E in the target material. The energy E is restricted to $E_{\text{p}} \geqq E \geqq E_{\text{p}} - \delta E_{\text{p}}$, where E_{p} and $E_{\text{p}} - \delta E_{\text{p}}$ are the energies of the projectile before and after passing through the target;

$V_{j\min}$ is then given implicitly by the expression

$$D_{\text{eff}} = M_j c^2 \int_{V_{j\min}}^{\bar{v}_j} \frac{V}{f(V)} \mathrm{d}V. \tag{A.34}$$

The γ-lineshape for a given projectile energy E and detection direction $\theta_\gamma \approx 0°$ can thus be obtained in good approximation from

$$\frac{\mathrm{d}n'(E, \Delta E'_\gamma, \theta_\gamma, \varphi_\gamma)}{\mathrm{d}E\,\mathrm{d}\Delta E'_\gamma \mathrm{d}\cos\theta_\gamma \mathrm{d}\varphi_\gamma} = \int_{\Delta E_1}^{\Delta E_2} g(\bar{v}_j(\Delta E_\gamma), V_j(\Delta E'_\gamma)) \left| \frac{\mathrm{d}V_j}{\mathrm{d}\Delta E'_\gamma} \right|$$
$$\times \left(\frac{E_{\gamma 0}+\Delta E'_\gamma}{E_{\gamma 0}+\Delta E_\gamma}\right)^2 \frac{\mathrm{d}n(E, \Delta E_\gamma, \theta_\gamma, \varphi_\gamma)}{\mathrm{d}E\,\mathrm{d}\Delta E_\gamma \mathrm{d}\cos\theta_\gamma \mathrm{d}\varphi_\gamma} \mathrm{d}\Delta E_\gamma, \tag{A.35}$$

where the integration is carried out over all ΔE_γ contributing to a given $\Delta E'_\gamma$. The function $V_j(\Delta E'_\gamma)$ is uniquely defined by eq. (A.32) with the exception of the small region $0 \leqq \cos\bar{\theta}_{\gamma j} \leqq \bar{v}_j/(1+0.5\bar{v}_j)$, where $V_j(\Delta E'_\gamma)$ is double valued. Here a linear interpolation formula was used. The initial lineshape dn is given by eq. (A.21). In writing eq. (A.35) we ignore the fact that the transformation of the γ-angles Θ_γ, ϕ_γ into the lab system depends slightly on the velocity of the nucleus at the moment of its decay [eqs. (A.10) to (A.12)], although we do take into account the change of the solid angle. It was verified that this is a very good approximation as long as the target thickness is less than 300–500 μg/cm^2.

The γ-lineshape, corrected for the finite target thickness, is then given by

$$\frac{\mathrm{d}N'(\Delta E'_\gamma)}{\mathrm{d}\Delta E'_\gamma} \propto \int_{E_\mathrm{p}}^{E_\mathrm{p}-\delta E_\mathrm{p}} \left(\frac{\mathrm{d}E}{\mathrm{d}(\rho x)}\right)_\mathrm{p}^{-1} \int_{\cos\theta_{\gamma\min}}^{\cos\theta_{\gamma\max}} e(\theta_\gamma) \frac{\mathrm{d}n'(E, \Delta E'_\gamma, \theta_\gamma, \varphi_\gamma = 0)}{\mathrm{d}E\,\mathrm{d}\Delta E'_\gamma \mathrm{d}\cos\theta_\gamma \mathrm{d}\varphi_\gamma} \mathrm{d}\cos\theta_\gamma \mathrm{d}E \tag{A.36}$$

for a detector located at $\theta_{\gamma 0} \approx 0°$. The specific energy loss of the projectile in the target material is $(\mathrm{d}E/\mathrm{d}(\rho x))_\mathrm{p}$.

Appendix B

PARAMETERIZATION OF INTRINSIC LINESHAPES OF Ge(Li) DETECTORS

The lineshape $g(E_0, E)$ observed in a Ge(Li) detector for monoenergetic γ-rays of energy E_0 was parameterized in the energy region between the photopeak E_0 and E_0-500 keV using a set of analytic functions,

$$g(E_0, E) = Q_0 \sum_{i=1}^{6} g_i(E_0, E).$$

In fig. 17 the synthesis of the lineshape is shown schematically. The six functions are

$$g_1(E_0, E) = Q_1 \left(\frac{4\ln 2}{\pi Q_3^2}\right)^{\frac{1}{2}} \exp\left[-(E-E_0)^2 4\ln 2/Q_3^2\right],$$

$$g_2(E_0, E) = Q_6 f(E) \exp\left[Q_7(E-E_0)\right],$$

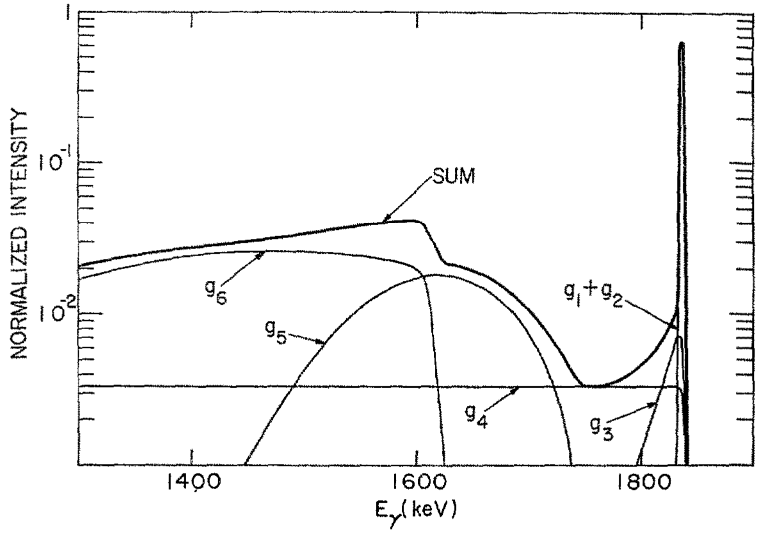

Fig. 17. Illustration of the synthesis of a lineshape observed in a Ge(Li) detector for monoenergetic γ-rays using the six functions g_i described in the text.

with

$$f(E) = \{1+Q_4 \exp[(E-E_0)2 \ln 9/Q_5]\}^{-1},$$

$$g_3(E_0, E) = Q_8 f(E) \exp[Q_9(E-E_0)],$$

$$g_4(E_0, E) = Q_{10} f(E),$$

$$g_5(E_0, E) = \max\left\{0, \left(\frac{4 \ln 2}{\pi Q_{13}^2}\right)^{\frac{1}{2}} [Q_{11}-Q_{14}(E-(E_0-Q_{12}))] \times \exp[-(E-(E_0-Q_{12}))^2 4 \ln 2/Q_{13}^2]\right\},$$

$$g_6(E_0, E) = Q_{15} \exp[Q_{18}(E-(E_0-Q_{16}))+Q_{19}(E-(E_0-Q_{16}))^2] \times \{1+\exp[(E-(E_0-Q_{16}))2 \ln 9/Q_{17}]\}^{-1}.$$

The intensity Q_1 is chosen in such a way that the area of the photopeak, defined by the sum of g_1 and g_2, is normalized to 1. The seventeen free parameters were determined by means of a non-linear least-squares fit.

As an example, the parameters obtained for a 30 cm^3 coaxial detector and several monoenergetic γ-rays are shown in fig. 18. Their dependence on E_0 is smooth. Therefore for a given energy E_0 the corresponding set of lineshape parameters can be easily interpolated using these curves.

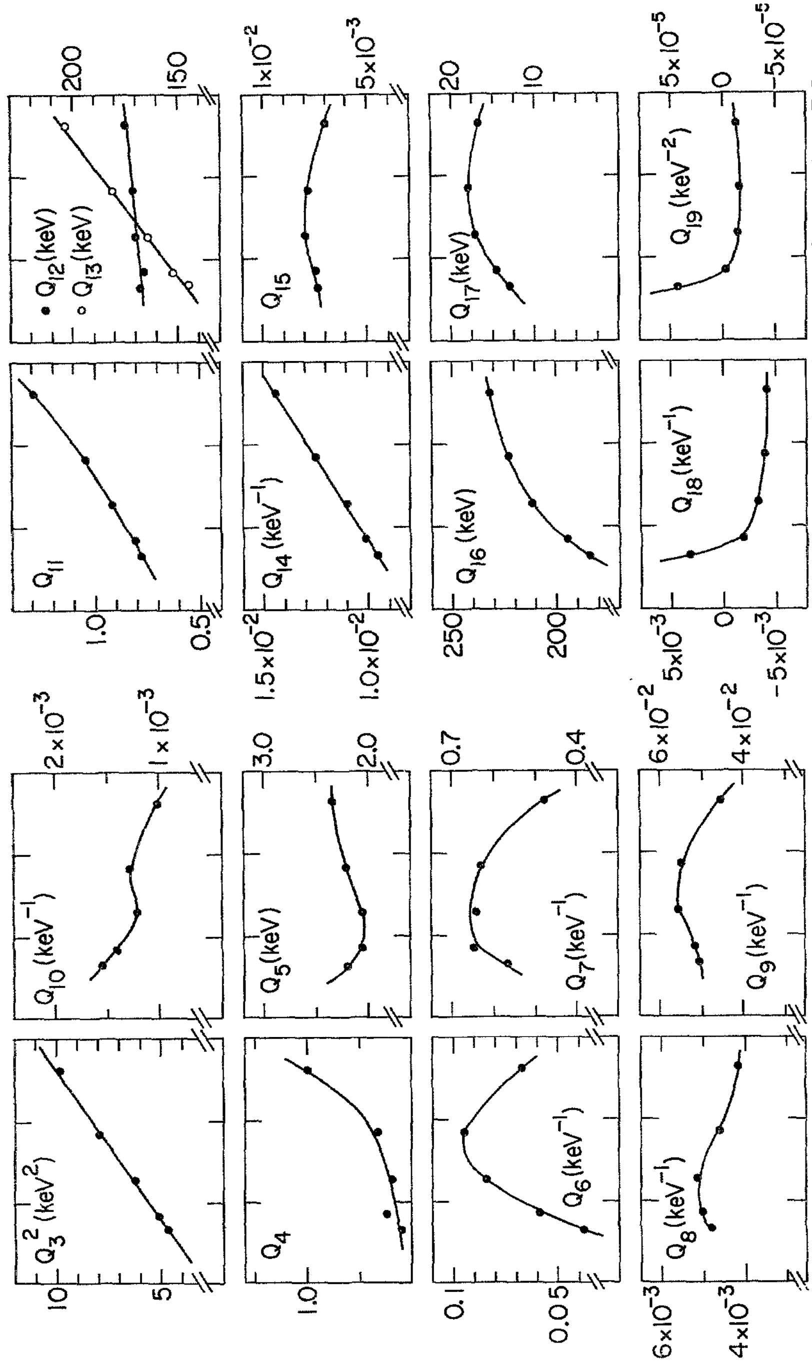

Fig. 18. Dependence of the 17 lineshape parameters Q_i on the γ-ray energy E_0 for a 30 cm^3 Ge(Li) detector.

References

1) G. Breit, R. L. Gluckstern and J. E. Russell, Phys. Rev. **103** (1956) 727
2) J. de Boer and J. Eichler, in Advances in nuclear physics, vol. 1, ed. M. Baranger and E. Vogt (Plenum Press, New York, 1968) p. 1
3) A. Bamberger, P. G. Bizzeti and B. Povh, Phys. Rev. Lett. **21** (1968) 1599;
D. Schwalm and B. Povh, Phys. Lett. **29B** (1969) 103
4) O. Häusser, B. W. Hooton, D. Pelte, T. K. Alexander and H. C. Evans, Phys. Rev. Lett. **22** (1969) 359; Can. J. Phys. **48** (1970) 35;
D. Pelte, O. Häusser, T. K. Alexander and H. C. Evans, Can. J. Phys. **47** (1969) 1929;
O. Häusser, T. K. Alexander, D. Pelte, B. W. Hooton and H. C. Evans, Phys. Rev. Lett. **23** (1969) 320;
D. Pelte, O. Häusser, T. K. Alexander, B. W. Hooten and H. C. Evans, Phys. Lett. **29B** (1969) 660;
D. L. Disdier, O. Häusser and A. J. Ferguson, Atomic Energy of Canada, Progress Report PR-P-89 (1971) p. 13
5) K. Nakai, F. S. Stephens and R. M. Diamond, Nucl. Phys. **A150** (1970) 114;
K. Nakai, J. L. Québert, F. S. Stephens and R. M. Diamond, Phys. Rev. Lett. **24** (1970) 903;
K. Nakai, F. S. Stephens and R. M. Diamond, Phys. Lett. **34B** (1971) 389
6) D. Vitoux, R. C. Haight and J. X. Saladin, Phys. Rev. **C3** (1971) 718
7) D. K. Olsen, W. R. Phillips and A. R. Barnett, Phys. Lett. **39B** (1972) 201
8) M. A. Fässler, B. Povh and D. Schwalm, Ann. of Phys. **63** (1971) 577
9) Z. Berant, M. B. Goldberg, G. Goldring, S. S. Hanna, H. M. Loebenstein, I. Plesser, M. Popp, J. S. Sokolowski, P. N. Tandon and Y. Wolfson, Nucl. Phys. **A178** (1971) 155
10) A. Winther and J. de Boer, in Coulomb excitation, ed. K. Alder and A. Winther (Academic Press, New York and London, 1966) p. 303
11) A. R. Poletti and E. K. Warburton, Phys. Rev. **137** (1965) B595
12) U. Smilansky, Phys. Lett. **25B** (1967) 385; Nucl. Phys. **A112** (1968) 185
13) K. Alder and H. K. A. Pauli, Nucl. Phys. **A128** (1969) 193
14) J. M. Wyckoff, B. Ziegler, H. W. Koch and R. Uhlig, Phys. Rev. **137** (1965) B576
15) N. MacDonald, Phys. Lett. **10** (1964) 334
16) H. Nebel and D. L. Lin, Phys. Rev. **156** (1967) 1133
17) A. C. Douglas and N. MacDonald, Phys. Lett. **24B** (1967) 447
18) W. H. Bassichis and F. Scheck, Phys. Rev. **145** (1966) 771
19) K. Nakai and A. Winther, unpublished
20) O. Häusser and R. Y. Cusson, Can. J. Phys. **48** (1970) 240
21) R. A. Eisenstein and U. Smilansky, Phys. Lett. **31B** (1970) 436
22) D. Cline, H. S. Gertzman, H. E. Gove, P. M. S. Lesser and J. J. Schwartz, Nucl. Phys. **A133** (1969) 445
23) D. Schwalm, G. A. P. Engelbertink, J. W. Olness and E. K. Warburton, to be published
24) E. Leischner, UNILAC-Report 1-66, Heidelberg (1966)
25) L. Grodzins, R. Kalish, D. Murnick, R. J. Van de Graaff, F. Chmara and P. H. Rose, Phys. Lett. **24B** (1967) 282
26) I. S. Dmitriev, and V. S. Nikolaev, JETP (Sov. Phys.) **20** (1965) 409
27) C. Scherer, Nucl. Phys. **A157** (1970) 81
28) M. Blume, Nucl. Phys. **A167** (1971) 81, and private communication
29) A. Abragam and R. V. Pound, Phys. Rev. **92** (1953) 943
30) D. Schwalm and B. Povh, to be published
31) O. Häusser, D. Pelte, T. K. Alexander and H. C. Evans, Can. J. Phys. **47** (1969) 1065
32) G. Schrieder, MPI Jahresbericht 1970, Heidelberg, 1970, and private communication
33) J. B. Marion, Nucl. Data **A4** (1968) 301
34) R. Gunnink, R. A. Meyer, J. B. Niday and R. P. Anderson, Nucl. Instr. **65** (1968) 26;
M. G. Strauss, F. R. Lenkszus and J. J. Eichholz, Nucl. Instr. **76** (1969) 285;
J. Kern, Nucl. Instr. **79** (1970) 233;
R. G. Helmer, R. C. Greenwood and R. J. Gehrke, Nucl. Instr. **96** (1971) 173;
Nucl. Data Sheets **B5** (1971) 205

35) P. Spilling, H. Gruppelaar, H. F. de Vries and A. M. J. Spits, Nucl. Phys. **A113** (1968) 395
36) E. A. Samworth, E. K. Warburton and G. A. P. Engelbertink, Phys. Rev. **C5** (1972) 138
37) P. Spilling, H. Gruppelaar and A. M. F. Op den Kamp, Nucl. Phys. **A102** (1967) 209
38) D. Goosman, private communication
39) D. H. White and D. J. Groves, Nucl. Phys. **A91** (1967) 453
40) P. M. Endt and C. van der Leun, Nucl. Phys. **A105** (1967) 1
41) J. A. Haskett and R. D. Bent, Phys. Rev. **C4** (1971) 461
42) D. Cline and P. M. S. Lesser, Nucl. Instr. **82** (1970) 291
43) C. P. Swann, Phys. Rev. **C4** (1971) 1489
44) T. K. Alexander, C. Broude, O. Häusser and D. Pelte, in Contributions to the Int. Conf. on nuclear states, Montreal, 1969, p. 137
45) S. J. Skorka, J. Hertel and T. W. Retz-Schmidt, Nucl. Data **A2** (1966) 347
46) K. W. Jones, A. Z. Schwarzschild, E. K. Warburton and D. B. Fossan, Phys. Rev. **178** (1969) 1773
47) M. A. Eswaran and C. Broude, Can. J. Phys. **42** (1964) 1311;
K. P. Lieb, Nucl. Phys. **85** (1966) 461;
D. Evers, Ph.D. thesis, Univ. of Hamburg, Germany, 1968
48) D. S. Andreyev, A. P. Grinberg, K. I. Erokhina and I. Kh. Lemberg, Nucl. Phys. **19** (1960) 400
49) O. Häusser, T. K. Alexander, A. B. McDonald, G. T. Ewans and A. E. Litherland, Nucl. Phys. **A168** (1971) 17
50) O. Häusser, private communication
51) W. Kutschera, D. Pelte and G. Schrieder, Nucl. Phys. **A111** (1968) 529;
D. Branford, N. Gardner and I. F. Wright, in Contributions to the Int. Conf. on nuclear states, Montreal, 1969, p. 112;
O. Häusser, T. K. Alexander and C. Broude, Can. J. Phys. **46** (1968) 1035;
A. E. Litherland, P. J. M. Smulders and T. K. Alexander, Can. J. Phys. **47** (1969) 639
52) D. Kurath, Phys. Rev. **C5** (1972) 768
53) E. C. Halbert, J. B. McGrory, B. H. Wildenthal and S. P. Pandya, in Advances in nuclear physics, vol. 4, ed. M. Baranger and E. Vogt (Plenum Press, New York, 1971) p. 316;
B. H. Wildenthal, J. B. McGrory and P. W. M. Glaudemans, Phys. Rev. Lett. **26** (1971) 96;
J. B. McGrory and B. H. Wildenthal, Phys. Lett. **34B** (1971) 373
54) M. R. Gunye, Phys. Lett. **37B** (1971) 125
55) G. H. Fuller and V. W. Cohen, Nucl. Data Tables **A5** (1969) 433
56) E. K. Warburton, J. W. Olness and A. R. Poletti, Phys. Rev. **160** (1967) 938
57) J. Lindhard, M. Scharff and H. E. Schiøtt, Mat. Fys. Medd. Dan. Vid. Selsk. **33**, No. 14 (1963)